ORGANIC PROCESS RESEARCH & DEVELOPMENT
OPR&D

pubs.acs.org/OPRD

Article

One-Pot Synthesis of Menthol from Citral over Ni/H-β-38 Extrudates Containing Bentonite Clay Binder in Batch and Continuous Reactors

Irina L. Simakova, Zuzana Vajglová, Mark Martínez-Klimov, Kari Eränen, Markus Peurla, Päivi Mäki-Arvela, and Dmitry Yu. Murzin*

Cite This: *Org. Process Res. Dev.* 2023, 27, 295−310

Read Online

ACCESS | Metrics & More | Article Recommendations | Supporting Information

ABSTRACT: Optimization of bifunctional Ni catalysts was performed to enhance the catalytic performance in the one-pot synthesis of commercially valuable menthol from citral. The effect of nickel precursors (nitrate, chloride, acetate, and sulfate) and the addition of bentonite clay was investigated in citral transformations in a batch reactor at 70 °C and 10 bar hydrogen, demonstrating higher activity for the Ni-H-β-38-bentonite composite derived from a nickel nitrate precursor, which can be attributed to a higher surface area, optimal Brønsted to Lewis acidity and metal particle size, as well as the egg-shell distribution of Ni particles. H-β-38 impregnated with nickel nitrate, followed by calcination and reduction, was shaped with bentonite as a binder to give extrudates for exploring the citral transformations in the trickle-bed reactor at 50−70 °C and 10 bar hydrogen. The highest selectivity to the desired menthols of 45% was obtained with 70% stereoselectivity to the menthol isomer at 70 °C. The apparent activation energy for citral transformations to menthols of 18.6 kJ/mol indicated the presence of mass transfer limitations. Catalytic activity was linked with the physical-chemical properties, which were characterized by transmission electron microscopy, X-ray diffraction, temperature-programmed reduction, Fourier transform infrared spectroscopy with pyridine, N_2 physisorption, and inductively coupled plasma−optical emission spectrometry methods.

KEYWORDS: *citral, menthol, shaped catalyst, clay binder, Ni precursors, trickle-bed*

INTRODUCTION

Catalytic hydrogenation of α,β-unsaturated aldehydes is an important reaction in the fine chemical industry. Synthesis of fine organic chemicals is typically a multistep process, for example, (−)-menthol is industrially produced by BASF starting from the enantioselective hydrogenation of nerol to (+)-citronellal, followed by its cyclization to (−)-isopulegol and further hydrogenation to (−)-menthol.[1,2] In the cases of citral and cinnamaldehyde, particularly, the nickel supported catalysts show a high selectivity for hydrogenation of the conjugated C═C double bond, while their activity for hydrogenation of the C═O bond to form unsaturated alcohols is rather low.[3,4] One-pot synthesis of menthols from citral (Scheme 1) has been extensively studied in the presence of noble (Pt, Pd, Ir) and non-noble (Ni, Co, Cu) metals in a batch reactor,[3−6] illustrating that Ni along with Pd was considered to be the most efficient for hydrogenation of citral and intermediate isopulegols to menthols. This reaction requires a bifunctional catalyst because in the first step citronellal is cyclized over Lewis acid sites,[7] and for hydrogenation of the formed isopulegol in the second step, the presence of a metal to dissociate hydrogen is needed. Metal ions with strong Lewis acidity facilitate the coordination of oxygen in the C═O group and the C═C double bond at C6 in citronellal onto, e.g., the zirconium ion in ZrO_2. Thereafter, citronellal is in a favorable orientation for ring closure via the intramolecular carbonyl-ene reaction. Oxygen protonates in the presence of the Brønsted hydroxyl group, and hydrogen abstraction occurs from the isopropyl group.[7]

The main scientific interest in this citral transformation is often limited to elucidation of activity, selectivity, and stability as well as the effect of reaction conditions and metal loading on menthol productivity. Other important factors affecting catalytic performance in general and selectivity for the competitive hydrogenation of conjugated C═C and C═O bonds in particular such as the type of metal precursor or mesoporous clay materials for zeolite shaping are rarely investigated. The effect of the nickel precursor on the surface properties of Ni/KL-supported catalysts prepared from nickel nitrate, nickel acetylacetonate, and nickel phthalocyanine was explored in hydrogenation of citral at 5 MPa and 50 °C, demonstrating different nickel species distribution in the zeolite and giving as the main reaction products always citronellal and citronellol.[8] The prominent effect of Ni precursors was demonstrated, however, for various processes, e.g., ammonia decomposition for the production of CO_x-free hydrogen (nickel nitrate, nickel acetylacetonate),[9] CO_2 methanation (nickel acetate, nickel nitrate, nickel acetylacetonate, nickel sulfate, and nickel chloride)[10] including over zeolite 5A and 13X supported catalysts (nickel nitrate, nickel citrate, and nickel acetate),[11] 1,1,1,2-tetrafluoroethane pyrol-

Received: October 25, 2022
Published: January 30, 2023

Scheme 1. Simplified Reaction Scheme for Citral Transformation to Menthols with Side Reactions[18]

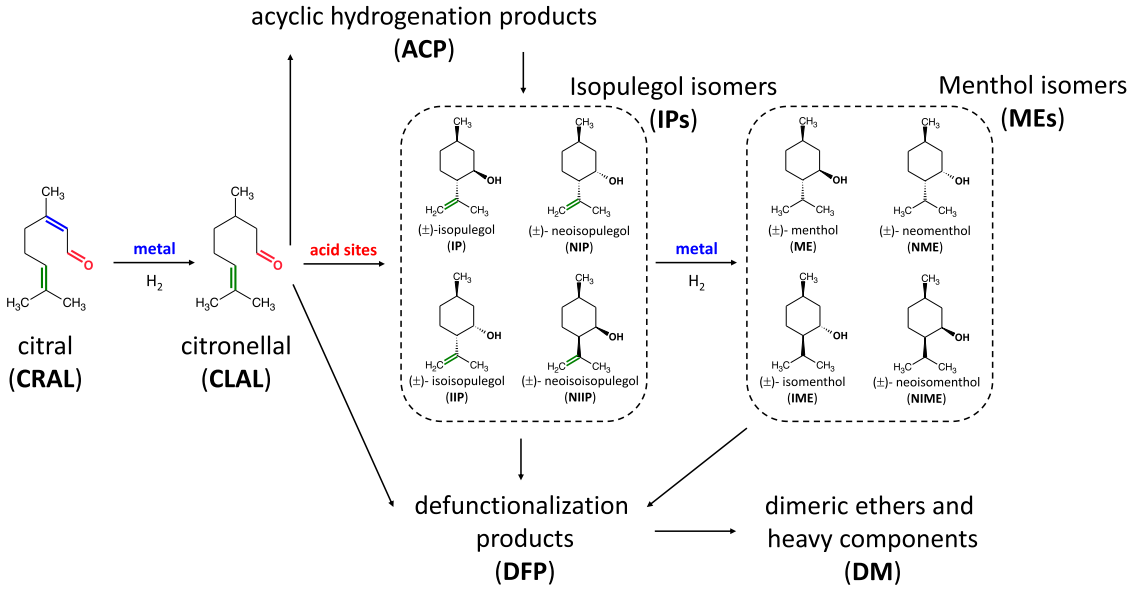

ysis to trifluoroethylene (nickel acetate, nickel nitrate, and nickel chloride),[12] steam and enhanced steam methane reforming (nickel acetate, nickel nitrate),[13] glycerol steam reforming (nickel nitrate, nickel chloride, nickel acetate, and nickel acetylacetonate),[14] hydroisomerization of *n*-decane (nickel nitrate, nickel acetylacetonate, and (triethylenediamine)-nickel nitrate),[15] hydrogenation and ring-opening of tetralin (nickel nitrate, nickel citrate),[16] where formation of different surface Ni^0 species, amount of acid sites, adsorption of coordinating anions, and Ni particles' distribution depending on precursors were shown to directly affect Ni dispersion and accessibility. Therefore, the choice of the metal salt precursor can also be significant when designing Ni-based catalysts for citral hydrogenation. Continuous operation compared to a batch mode facilitates economically feasible production if the catalyst is selective and stable enough. Continuous mode requires the use of shaped catalysts, where scale-up is typically not straightforward, also considering that the initial catalyst screening is performed typically in the kinetic regime, while continuous operation involves mass transfer limitations influencing not only activity but also selectivity. In particular, it was recently shown that in the one-pot synthesis of menthol different product distributions was obtained with the same catalyst in the powder and extrudate forms under similar conditions in batch and continuous reactors, respectively.[17] Several binders including inexpensive clays,[17−19] silica,[20] and alumina[21] have been used for preparation of extrudates. One-pot synthesis of menthol was investigated in particular using Ni supported on H-β-38 with either sepiolite[22] or attapulgite[23] as binders. Furthermore, sepiolite was used as a binder for Ni/mesoporous aluminosilicate in the same reaction.[2] Different preparation methods for extrudates were used to tune the metal location. When Ni was deposited exclusively on a clay binder, the results were less promising compared to nickel deposition on either β zeolite or its mixture. Furthermore, the catalyst characterization revealed large changes in textural and acidic properties among these extrudates. In addition, it has been shown that in some cases the binder is not inert, interacting with the support.[24] Previous experience with other binders (bentonite, bleaching earth, attapulgite, and sepiolite) for the citronellal cyclization demonstrated that introduction of different clays gives different Si/Al ratios, acidity, textural properties of the composites, and thereby activity and selectivity to isopulegols,[19] which was difficult to predict for much more complex one-pot synthesis of menthol. Ni/H-β-38 composite catalysts containing attapulgite[23] and sepiolite[22] as binders were earlier used in the one-pot synthesis of menthol from citral, demonstrating different catalytic behaviors.

In the current work, bentonite, a clay composed of montmorillonite and kaolinite phases as well as hematite,[25] was applied as a binder; besides these phases, K, Mg, and Fe are present as impurities in ca. 1, 1, and 2 wt %.[19] Bentonite also contains several other elements as impurities, e.g., Ca, Na, S, Ti, and Cl.[26,27] Furthermore, to elucidate the role of the metal precursor, several nickel precursors (acetate, nitrate, sulfate, and chloride) were used to synthesize powder catalysts containing H-β-38 modified with bentonite as a support (the number 38 denotes the SiO_2/Al_2O_3 ratio). These samples were characterized and tested in citral transformations to take the best advantage of the support material. Based on the results obtained in a batch reactor, the best-performing powder catalyst containing nickel nitrate as a precursor was selected for further studies using Ni/H-β-38 and bentonite as a binder to prepare a cylindrically shaped catalyst. This catalyst was tested in a trickle-bed reactor for citral transformation and, along with powdered catalysts, was characterized by TEM, XRD, TPR, FTIR with pyridine, ICP-OES, and N_2 physisorption methods to find a correlation with catalyst performance. In addition, the activity of the bentonite containing Ni-H-β-38 composite was compared with the counterpart catalytic materials containing sepiolite and attapulgite under similar reaction conditions.

RESULTS AND DISCUSSIONS

Catalyst Characterization. To investigate the microstructure of the Ni/(H-β-38+bentonite) catalysts prepared from different precursors (where ex-nitrate, ex-acetate, ex-chloride, and ex-sulfate samples are denoted as NiN, NiA, NiC, and NiS, respectively), as well as ex-nitrate extrudates of a similar composition [(Ni/H-β-38)+bentonite] and ex-nitrate

https://doi.org/10.1021/acs.oprd.2c00337
Org. Process Res. Dev. 2023, 27, 295−310

bentonite-free Ni/H-β-38, they were studied by transmission electron microscopy (TEM), high-angle annular dark-field scanning transmission electron microscopy (HAADF-STEM), and EDX mapping (Figures S1−S4). Figure S1 shows results for both fresh and spent NiN catalysts, Figure S2 presents micrographs for fresh and spent NiS catalysts, and Figure S3 displays images for fresh NiA and NiCl catalysts, respectively. TEM images and histograms for ex-nitrate extrudates and ex-nitrate bentonite-free Ni/H-β-38 catalysts before and after reaction are presented in Figure S4, allowing one to estimate the average Ni particle size, their distribution, and evolution under reaction conditions. The results related to spent catalysts are discussed in the sections related to activity and selectivity in batch and trickle-bed reactors. TEM images (Figures S1−S4) show that H-β-38 particles exhibit a round-shaped structure and that Ni particles predominantly of a spherical form are well dispersed on it.

Figures S1d,f presents an overlay map of the Ni, Al, and Si chemical distributions for the fresh reduced NiN catalyst. These mapping data clearly show that Ni nanoparticles form an egg-shell structure from the ex-nitrate zeolite−bentonite mixture, which was not observed for other precursors. According to HAADF-STEM-EDX mapping, fresh NiS catalysts contained ca. 2−3 wt % sulfur, depending on the selected location on the surface, when Al, Si, Ni, and S were normalized to 100% (Figure S2g,j). This result demonstrates that the residual sulfur content remained the same in the fresh case. Note that the ex-chloride catalyst is characterized by the presence of a large fraction of agglomerated nanoparticles along with separately located large Ni crystals (Figure S3e,f), indicating a rather low metal surface not allowing a reliable statistical analysis. In the case of ex-acetate, well-distributed small spherical nanoparticles were observed (Figure S3a−d). Analysis of the average Ni particle sizes (Table 1) shows that

Table 1. Average Ni Particle Size (d_{Ni}) and Dispersion (D%) of Fresh Ni/H-β-38 Catalysts Based on TEM[a]

catalyst	d_{Ni}, fresh catalyst (nm)	d_{Ni}, spent catalyst (nm)	dispersion (D%) of fresh catalysts
5 wt % Ni/H-β-38, bentonite-free, P	6	7	16.2
11 wt % NiN P	11	12	8.8
11 wt % NiA P	6	n.d.	16.2
11 wt % NiS P	2	3	48.6
11 wt % NiCl P	n.d.	n.d.	n.d.
5 wt % [(NiN/H-β-38) + bentonite] E	10	16	n.d.

[a]Notation: N, from nitrate; A, from acetate; S, from sulfate; Cl, from chloride; P, powder catalyst; E, extrudate.

the smallest Ni particles were present in NiS followed by NiA and bentonite-free Ni/H-β-38, with the same Ni particle size for the latest two materials, while the largest Ni particles with the size of 11 nm were present in NiN. Similarly, Wu et al.[14] reported that according to TEM NiA and NiN catalysts had Ni particles uniformly dispersed over alumina and distributed within a narrow size range, while NiC had a larger Ni particle size and a broader distribution range. The 2-fold larger mean Ni particle size in the 11 wt % NiN catalyst compared to the 5 wt % Ni/H-β-38_P (in which P denotes powder) prepared from a similar Ni precursor could be related to the ca. 2-fold higher metal loading probably resulting from an increasing metal surface density favoring Ni particle growth.[28] The fibers present in bentonite[18] were clearly visible in extrudates, which were shaped from bentonite powder and Ni/H-β-38 (Figure S4). When Ni was loaded on the mixture of H-β-38 and bentonite, the structure became more homogeneous and the separate bentonite phase could not be seen (Figures S1−S3). The Ni dispersion (D%) in Ni/H-β-38 catalysts calculated from the average metal particle sizes, d_{Ni}, are shown in Table 1.

The textural properties of fresh and some spent Ni catalysts were determined by nitrogen adsorption (Table 2) focusing on mesostructural features, which are more important in catalytic liquid-phase hydrogenation of bulk organic molecules. The textural properties of the initial H-β-38 and bentonite are given in Table 2 (entries 1, 2) as a comparison. The bentonite used in the current work was found to exhibit a BET specific surface area of 172 m^2/g, while bentonite from Brazil and Morocco exhibited only 25[26] and 83 m^2/g,[27] respectively. H-β-38 is a microporous zeolite, while bentonite exhibits predominantly mesopores and a lower specific surface area in comparison to the H-β-zeolite. As mentioned above, introduction of the binder was, however, necessary for shaping the zeolite through extrusion. The BET specific surface area of bentonite-free 5 wt % Ni/H-β-38 was 330 m^2/g_{cat} (Table 2, entry 3). Data for catalysts prepared from different nickel precursors and (H-β-38+bentonite) mixture with mass ratio 7/3 as a support are given in Table 2, entries 5−8.

The specific surface area observed for the powder catalysts prepared from different Ni precursors and supported on a mixture of H-β-38 and bentonite exhibited different specific surface areas varying in the range of 213 to 299 m^2/g_{cat}, with the highest specific surface area observed for the ex-nitrate catalyst (NiN), while the lowest one was recorded for the ex-acetate catalyst (NiA). This result demonstrates that the selection of the metal precursor is very important.

Powder X-ray diffraction patterns of [Ni/(H-β-38) + bentonite] extrudates after calcination and reduction before and after the reaction are presented in Figure 1. The fresh calcined reduced extrudates contain reflexes from the β-zeolite (PDF No. 00-056-0487) as well as from Ni^0 (PDF No. 04-0850) with the determined value of the lattice parameter a = 3.524 Å and average coherently scattering domain (CSD) size D_{Ni} = 18.0 nm, as well as low intensive peaks of the nickel oxide phase NiO (PDF No. 047-1049, $a = b = c$ = 4.177 Å) with average CSD size D_{NiO} = 10.0 nm. It is important to note that the β-zeolite structure was not changed during catalyst preparation (Figure 1a). The results related to the XRD of the spent catalysts are discussed in the section Activity and Selectivity in a Trickle-Bed Reactor.

The Brønsted and Lewis acidities of different materials, e.g., the catalysts, the binder, and the support, are reported in Table 3. The molar SiO_2/Al_2O_3 ratio of the bentonite used in the current study was 9 (Table 3, entry 7),[19] indicating that it is rather acidic. However, it contained only weak and medium Brønsted acid sites with a BAS/LAS ratio of 2, while for H-β-38 it was close to 9 (Table 3, entry 6). The H-β-38-bentonite powder mixture (Table 3, entry 9) exhibited a lower BAS/LAS ratio than the theoretically calculated one based on the acidities of separate raw materials, i.e., H-β-38 and bentonite (Table 3, entry 8). This result shows that the acidities are not directly additive (Table 3, entries 8 and 9), as also observed previously for sepiolite[22] and attapulgite[22] containing H-β-38 catalysts. Ni supported only on H-β-38 exhibited a high amount of weak and medium Brønsted acid sites with, however, its BAS/LAS ratio of only 0.6 (Table 3, entry 1).

https://doi.org/10.1021/acs.oprd.2c00337
Org. Process Res. Dev. 2023, 27, 295−310

Table 2. Textural Properties of Catalysts[a]

entry	sample	S_{BET} m^2/g	$V_{m,BJH}$ cm^3/g	$S_{D\text{-}R}$ m^2/g	V	V_μ cm^3/g	V_m	V_m/V_μ
1	H-β-38	375	0.13	589	0.3	0.23	0.08	0.31
2	bentonite	172	0.26	202	4.0	0.05	0.20	0.25
3	5 wt % NiN/H-β-38, bentonite-free, fresh P	330	0.13	513	0.4	0.21	0.08	0.29
4	5 wt % NiN/H-β-38, bentonite-free, spent P	129	0.11	194	0.8	0.08	0.06	0.14
5	11 wt % NiN P	299	0.22	n.d.	n.d.	n.d.	n.d.	n.d.
6	11 wt % NiS P	229	0.17	n.d.	n.d.	n.d.	n.d.	n.d.
7	11 wt % NiA P	213	0.20	n.d.	n.d.	n.d.	n.d.	n.d.
8	11 wt % NiCl P	271	0.17	n.d.	n.d.	n.d.	n.d.	n.d.
9	11 wt % NiN spent P	136	0.16	n.d.	n.d.	n.d.	n.d.	n.d.
10	11 wt % NiS spent P	75	0.15	n.d.	n.d.	n.d.	n.d.	n.d.
11	5 wt % [(NiN/H-β-38) + bentonite], fresh E	272	0.21	418	0.9	0.17	0.15	0.32
12	5 wt % [(NiN/H-β-38) + bentonite], spent E	182	0.21	233	1.7	0.09	0.15	0.24

[a]Notation: S_{BET}, specific surface area calculated by the Brunauer−Emmett−Teller method; $V_{m,BJH}$, mesopore volume determined by the BJH method; $S_{D\text{-}R}$, specific surface area calculated by the Dubinin−Radushkevich method; V, total pore volume; V_μ, micropore volume; V_m, mesopore volume determined by the DFT method; N, from nitrate; A, from acetate; S, from sulfate; Cl, from chloride; P, powder; E, extrudate; n.d., not determined.

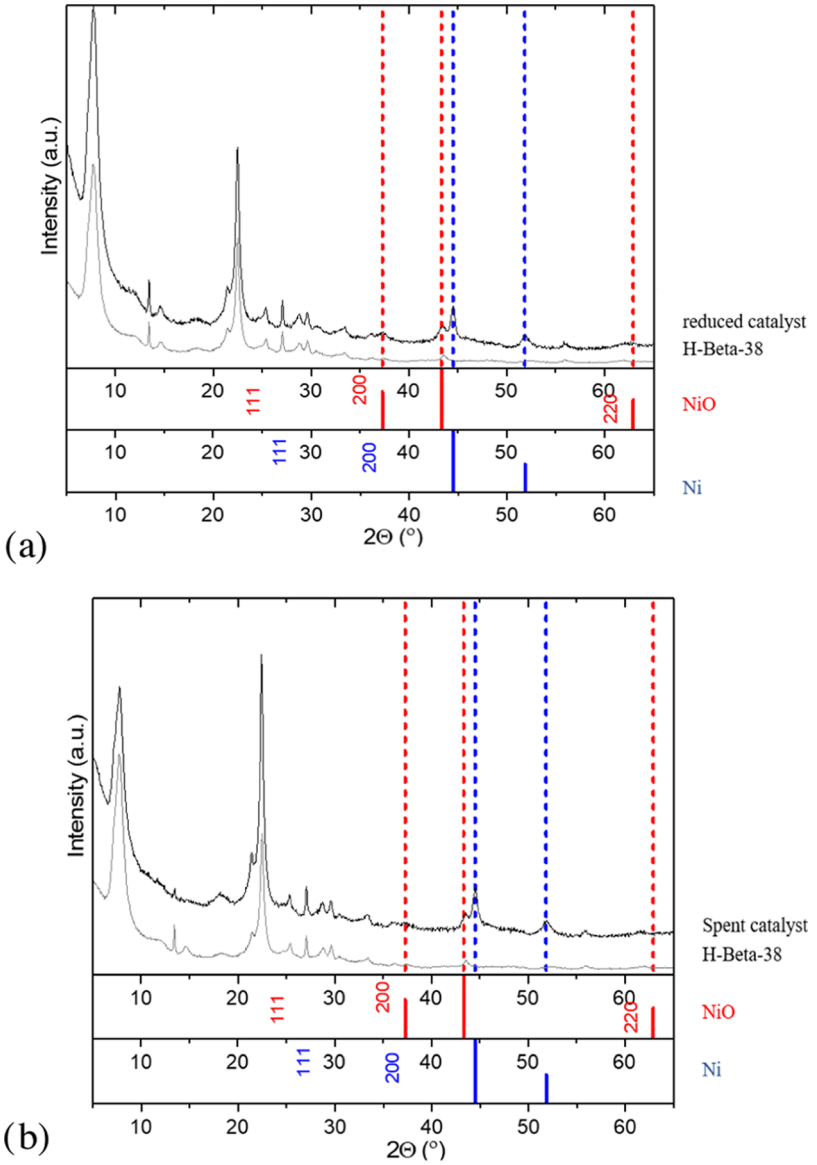

Figure 1. XRD patterns of calcined reduced (Ni/H-β-38) + bentonite extrudates compared to the initial H-β-38 zeolite: (a) fresh, (b) spent.

https://doi.org/10.1021/acs.oprd.2c00337
Org. Process Res. Dev. 2023, 27, 295−310

Table 3. Acidities Determined by FTIR Pyridine Adsorption−Desorption[a,b]

		weak (μmol/g)			medium (μmol/g)			strong (μmol/g)			total (μmol/g)			
entry	catalyst	BAS	LAS	total	BAS	LAS	total	BAS	LAS	total	BAS	LAS	total	BAS/LAS
1	5 wt % Ni/H-β-38 P	8	77	85	107	112	219	1	8	9	116	198	313	0.6
2	NiN P	60	45	105	96	30	126	0.4	0.2	0.6	156	74	230	2.1
3	NiS P	0	81	81	34	77	111	69	32	101	103	190	293	0.5
4	NiA P	25	72	97	67	55	122	15	7	22	107	134	241	0.8
5	NiCl P	8	49	57	56	33	89	26	15	41	90	97	187	0.9
6	H-β-38	18	19	37	40	10	50	221	2	223	279	31	310	9.0
7	bentonite P	16	14	30	20	5	25	0	0	0	36	19	54	2
8	calculated H-β-38 + bentonite(7/3 wt/wt)	17	17	35	34	8.5	43	155	1.4	156	206	27	233	6.9
9	H-β-38+bentonite P	22	24	46	18	5	22	116	10	125	155	38	193	4.1
10	(Ni/H-β-38)+bentonite E	0	79	79	123	54	177	4	13	17	128	145	273	0.9
11	[Ni/(H-β-38+bentonite)] E	8	85	93	27	32	59	67	67	133	101	184	286	0.5
12	[Ni/(H-β-38+attapulgite)] E	13	96	109	19	33	52	35	26	61	67	155	222	0.4
13	[Ni/(H-β-38+sepiolite)] E	26	90	116	39	30	71	21	22	43	86	144	230	0.6

[a]Notation: Reduction 450 °C, 4 h, 2 °C/min, N, from nitrate; A, from acetate; S, from sulfate; Cl, from chloride; P, powder; E, extrudate. [b]The acidity values were calculated from the acidity values of pure H-β-38 and pure bentonite, taking into account their weight fraction.

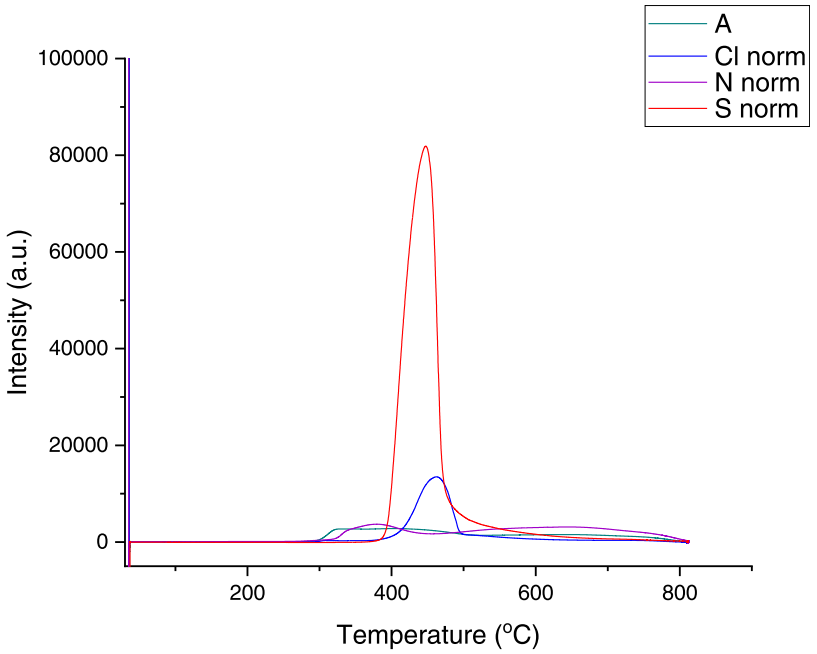

Figure 2. TPR of Ni catalysts prepared from different precursors. Catalysts NiN, NiA, and NiS were calcined before TPR, and NiCl was not calcined before TPR.

Table 3 clearly illustrates that the acidity of the catalysts when nickel was deposited from different precursors was clearly different from the acidity of the parent zeolites, which can be explained by a partial blocking of the Brønsted acid sites and generation of Lewis acid sites. Particularly interesting is the substantial decline in the number of strong Brønsted acid sites after metal introduction, which was reported previously for metal supported zeolites.[30,31] Moreover, the nature of the counterion in the precursor (e.g., chloride, nitrate, or acetate) also influenced not only the overall acidity but also the BAS/LAS ratio as well. It can be tentatively speculated that chloride and sulfate ions are more strongly adsorbed on the catalyst surface, being well-known catalyst poisons. An interesting observation from Table 3 is that both catalysts prepared from nickel nitrate, i.e., 5 wt % Ni/H-β-38 and NiN, have low amounts of strong BAS and LAS; moreover, the former catalyst has the largest amount of acid sites of medium strength, which could be essential for catalytic performance. Too high amounts of weak sites will inevitably lead to poor activity, while excessive concentrations of strong acids sites in the case of citral transformations to menthol can apparently promote side reactions. Utilization of nickel acetate and subsequent thermal treatment can lead to formation of acetic acid, which apparently influences the acidity of the supported catalyst in a milder way than nickel nitrate decomposing to easily release to the gas-phase NO_x.

The extrudates used in the current study for citral transformations were prepared by loading ex-nitrate Ni on H-β-38 and then extruding the paste with bentonite (Table 3, entry 10), which exhibited the BAS/LAS ratio of 0.9 and a very low amount of strong Brønsted acid sites. As a comparison, in the extrudates for which Ni was loaded both on H-β-38 and on

https://doi.org/10.1021/acs.oprd.2c00337
Org. Process Res. Dev. 2023, 27, 295−310

bentonite (Table 3, entry 11), the concentration of strong Brønsted acid sites was nearly 17-fold higher compared to [(Ni/H-β-38)+bentonite] (Table 3, entry 10), while the latter demonstrated a 4.5-fold higher concentration of medium Brønsted acid sites and did not contain weak Brønsted acid sites. This result clearly shows that the method of Ni introduction in extrudates plays an important role in formation of BAS and LAS with different strengths defining catalyst properties. Furthermore, as in our previous studies, [Ni/(H-β-38 + sepiolite)][22] (Table 3, entry 13) and [Ni/(β-38 + attapulgite)][23] (Table 3, entry 12) were applied as catalysts in citral transformations; their acidity is also given in Table 3 (entries 12, 13) for comparative purposes, indicating a lower total and BAS fraction compared to bentonite containing Ni/H-β-38 (Table 3, entries 10, 11). Their catalytic behavior reported earlier[22,23] will be compared further with that of bentonite containing Ni/H-β-38 explored in the current work.

Temperature-programmed reduction of the catalysts was carried out to determine differences in the reducibility of the Ni/(H-β-38 + bentonite) catalysts prepared with different precursors, related to the location and dispersion of nickel species after calcination, and the metal−support interactions based on comparison of the TPR profiles for the catalysts and unsupported nickel oxide taken from the literature. Corresponding Ni precursors were supported on the mixture of H-β-38 and bentonite and thereafter calcined in the cases of NiN, NiA, and NiS samples. The results from TPR experiments are presented in Figure 2 and Table 4. Figure 2 shows the TPR profiles of the preliminarily calcined NiN, NiA, and NiS and noncalcined NiCl samples. The TPR profiles of calcined NiN and NiA are very similar, exhibiting two broad nonsymmetrical reduction peaks with the T_{1max} at 377 and 325 °C and T_{2max} at 652 and 414 °C, respectively, probably corresponding to reduction of two types of oxidized nickel species in different positions in the zeolite framework. The first one could be at the outer surface being more easily reducible and the second one inside the channels interacting with the walls. Contrary to ex-nitrate and ex-acetate samples, the temperature-programmed reduction profiles of noncalcined ex-chloride and calcined ex-sulfate show a similar single reduction peak with the maximum at 462 and 448 °C (Figure 2), respectively, indicating the presence of one type of Ni species on the surface, which were reduced in just one step. Note that the maximum for the reduction temperature in the case of unsupported nickel oxide was reported to be 285 °C.[14] The TPR profiles of the catalysts prepared from different metal precursors are shifted to higher temperatures compared to the unsupported nickel oxide, which evidences stronger metal−support interactions as described below. Two reduction peaks were observed in TPR-H_2 for the ex-nitrate Ni/H-β catalyst, which displayed hydrogen consumption peaks at 400 and 620 °C although the metal loading was very low compared to NiN in this work.[34] The first reduction peak was related to NiO reduction, whereas the second one was assigned to the reduction of less reducible stabilized Ni^{2+} species located on zeolite sites,[34] in line with the current work. For both NiA and NiN, maximum hydrogen consumption in TPR was observed at relatively low temperatures, in line with the literature data.[32] According to these data, the maxima of the hydrogen consumption peak for nickel nitrate, acetate, sulfate, and chloride supported on alumina appeared at 395, 444, 463, and 505 °C, respectively.[32] Note that for the NiN TPR profile the peak at T_{1max} could be related to the reduction of NiO to Ni^0, while the reduction peak at a higher temperature (T_{2max}) can be assigned to the nickel-aluminum oxide species derived from stronger interactions between NiO and Al_2O_3, indicating the potential formation of a spinel structure of $NiAl_2O_4$.[33]

The area for desorbed hydrogen increased as follows: NiS > NiCl > NiN > NiA (Table 4). Because sulfur was confirmed to be present in the fresh and spent NiS catalysts by STEM-HAADF-EDX analysis (Figure S2g,j), the large hydrogen consumption is related not only to metal reduction but also to the partial reduction of sulfur in the sulfate, and thus, this hydrogen area detected by the TC detector cannot be correlated directly to the catalytic data. Furthermore, $NiSO_4$ has a high decomposition temperature,[35] indicating that a part of Ni is still chemically bonded to sulfur. $NiCl_2$ also has a high decomposition temperature;[36] it even demonstrated a high consumption of hydrogen in TPR up to 450 °C assuming that part of the absorbed hydrogen interacted with residual surface chlorine species. NiN exhibits the lowest decomposition temperature[37] among the studied Ni salts followed by NiA[38] although the lowest temperature for hydrogen consumption was observed for NiA followed by NiN (Table 4).

The mechanical strength of [(NiN/H-β-38) + bentonite] extrudates in the vertical and horizontal positions were 2.6 ± 0.3 and 1.2 ± 0.2 MPa, respectively (Table S1, entry 1). These values are low compared to the vertical and horizontal mechanical strengths of extrudates made only from bentonite in the presence of methylcellulose of 11.8 and 3.6 MPa,[39] respectively (Table S1, entry 3). At the same time, the results are on the same order of magnitude as those obtained for the ex-nitrate zeolites such as H-β-38 and H-β-25, extruded with attapulgite[23] (Table S1, entry 2) or bentonite (Table S1, entry 7), respectively, in the ratio of 7/3, exhibiting similar width and length and marginally changing after nickel insertion (Table S1, entries 2 and 6).[39] Note that bentonite extrudates as such demonstrated a rather high mechanical resistance to crushing, similar to attapulgite being more stable than a sepiolite (Table S1, entries 3−5).

Activity and Selectivity of Powder Ni/H-β-38 in Batch Experiments. The effect of the nickel precursor in the Ni/H-β-38-bentonite powder catalyst was investigated in the batch reactor performing citral hydrogenation at 70 °C and 10 bar hydrogen (Figures 3 and 4, Table 5). As a comparison, the performance of bentonite-free Ni/H-β-38 under comparable reaction conditions was also investigated. Kinetics of citral transformations over four different [Ni/(H-β-38 + bentonite)] powder catalysts is depicted in Figure 3a. Citral transformation

Table 4. Maximum Temperatures (T_{max}) for Hydrogen Consumption and Area of Hydrogen Consumed Calculated per Catalyst Mass in TPR for the Calcined Powder Catalysts[a]

catalyst	TPR up to 800 °C after calcination at 450 °C		TPR after calcination at 450 °C and reduction up to 450 °C			decomposition temperature of the salt (°C)
	$T_{1\,max}$ (°C)	$T_{2\,max}$ (°C)	$T_{1\,max}$ (°C)	$T_{2\,max}$ (°C)	area (a.u.)	
NiA	325	414	326	452	2.4×10^7	400−440[38]
NiCl[b]	462		452	n.d.	3.3×10^7	590[36]
NiN	377	652	369	n.d.	2.7×10^7	250[37]
NiS	448		426	n.d.	2.2×10^8	658[35]

[a]N.d., not detected. [b]Not calcined at 450 °C, only reduced.

https://doi.org/10.1021/acs.oprd.2c00337
Org. Process Res. Dev. 2023, 27, 295−310

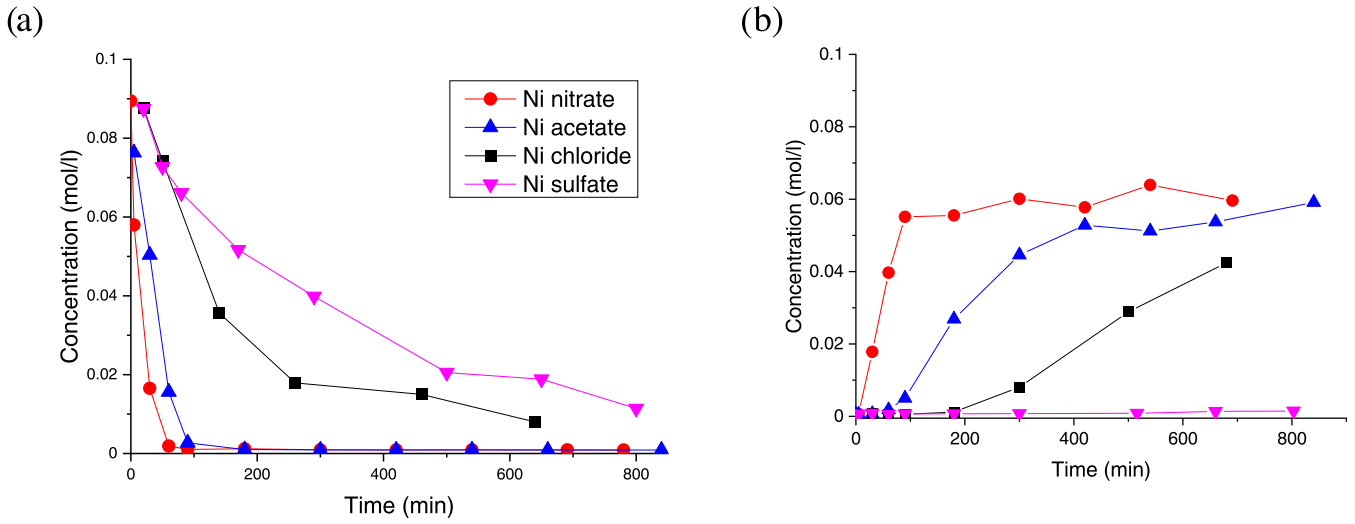

Figure 3. Kinetics of (a) citral transformation and (b) menthol formation over 11 wt % [Ni/(H-β-38+bentonite)] powder depending on Ni precursors (red circle, Ni nitrate; up triangle, Ni acetate; black square, Ni chloride; down triangle, Ni sulfate). Conditions: 70 °C, total pressure 11 bar, initial citral concentration 0.09 mol/L.

occurred most rapidly with NiN followed by NiA > NiCl ≫ NiS. The initial reaction rates were not correlating directly with the metal particle size because besides metal catalyzed hydrogenation also acid catalyzed hydrogenolysis occurred. The initial rates were calculated by dividing the initial conversion of citral by the time interval and the mass of nickel. Very low initial rates were determined for Ni/H-β-38-bentonite prepared from $NiCl_2$ and $NiSO_4$. Note that the performance of ex-nitrate bentonite-free Ni/H-β-38 differing by exclusively microporous microtexture (Table 2, entry 3) was characterized by low citral conversion (Table 5). Furthermore, when this catalyst was used in citral transformation to menthol, its specific surface area decreased by 61% due to extensive accumulation of organic materials on the catalyst surface (Table 2, entry 4). On the other hand, one reason for the low activity of ex-sulfate and ex-chloride catalysts could be the lowest volume of mesopores (Table 2, entries 6 and 8). Moreover, despite a large amount of hydrogen being consumed in TPR-H_2, most probably not all Ni species were in the reduced state (Table 4). On the other hand, ex-nitrate Ni/H-β-38-bentonite characterized by a higher surface area and a rather developed mesoporous structure (Table 2, entry 5) was very active (Figures 3 and 4b), with Ni being located predominantly at the outer surface of the catalyst, benefiting access to catalytically active metal sites (Figure 3g). The lowest activity of NiS (Table 5) is partially caused by the presence of sulfur in both the fresh and spent catalysts, with its content remaining constant during the reaction (Figure S2g,j). Thus, it is expected that sulfur can interact with organic molecules, provoking potentially severe catalyst deactivation.

A comparison of the reaction rates after prolonged reaction time shows that the catalysts prepared from nitrate and acetate were very active, giving complete conversion of citral at 180 and 300 min, respectively, while the NiCl catalyst gave only 91% conversion at 680 min (Figure 4a–c), which can be caused by the presence of large Ni particles (Figure S3e,f), which are catalytically inactive due to a low number of exposed sites. The NiS catalyst was rather inactive (Figure 4d). The bentonite-free microporous Ni/H-β-38 with the lowest surface area deactivated rapidly after 20 min (Figure 4d). Comparison of the catalytic behavior of ex-nitrates Ni/H-β-38-bentonite and bentonite-free Ni/H-β-38 powder catalysts allowed one to conclude that introduction of mesoporous bentonite allowed formation of the catalyst pore structure with sufficient mesoporosity and exposed Ni particles, whereas acidic properties of the zeolite were kept optimal for enabling one-pot citral transformations into menthols. Furthermore, TEM images of the spent catalysts (Figure S2) revealed that only a slight Ni agglomeration occurred during the reaction due to a low reaction temperature in the batch reactor with powder catalysts. However, the Ni particle size for ex-nitrate [(Ni/H-Beta38)+bentonite] extrudates exploited in citral transformation in a trickle-bed reactor with totally 19 h TOS increased from 10 to 16 nm, reflecting moderate nickel agglomeration during the reaction (Figure S4c,d).

The origin of catalyst deactivation can also be related to a decrease of the specific surface area for the spent catalysts. The specific surface areas for spent NiN and NiS catalysts were also recorded, showing that they decreased by 55% for NiN and 67% for NiS. In addition, 5 wt % NiN supported on H-β-38 and extruded with bentonite (Table 2, entry 11) has a somewhat lower specific surface area than the powdered catalyst with 11 wt % Ni (Table 2, entry 5) but a higher specific surface area compared to powdered NiS, NiA, and NiC catalysts. A similar decrease of both specific surface areas and the total pore volume was observed during α-pinene isomerization over gold on alumina, accompanied by a decrease in terpene conversion.[28] A study of the spent catalyst by TPO with MS analysis of oxidation products showed that predominantly organic deposits caused the catalyst deactivation because of formation of oligomers on the surface with the composition $(C_{10}H_{16})_x$.[29] Transformations of citral resulted in the formation of various unsaturated intermediates (Scheme 1) that also were prone to forming condensation products, negatively affecting catalytic activity.

Selectivity to different products was compared over different Ni/H-β-38-bentonite catalysts at 90% conversion and after 660 min (Table 5), although the corresponding values for Ni/H-β-38 are reported at the final conversion of 35%. The highest selectivity to menthols (70%) was obtained over NiN (Table 5), characterized by a rather high BAS/LAS ratio of 2.1 (total

https://doi.org/10.1021/acs.oprd.2c00337
Org. Process Res. Dev. 2023, 27, 295−310

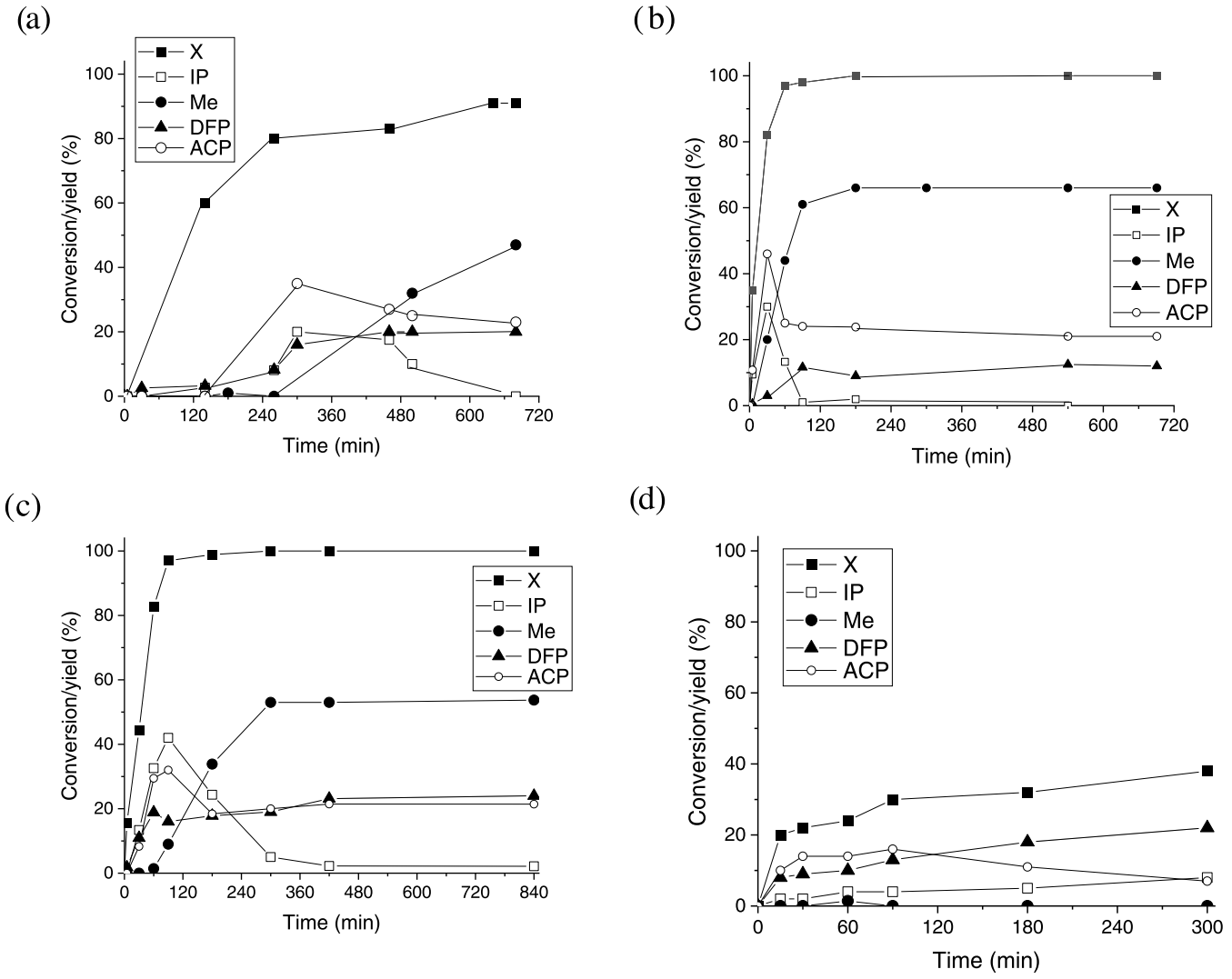

Figure 4. Conversion and product yield in citral transformations to menthols over 11 wt % [Ni/(H-β-38 + bentonite)] powder, in which the nickel precursor is (a) chloride, (b) nitrate, and (c) acetate and (d) bentonite-free 5 wt % Ni/H-β-38 in a batch reactor. Conditions: 70 °C, total pressure 11 bar, initial citral concentration 0.09 M, in (d) 10 bar. Notation: X, conversion; IP, pulegols; Me, menthol; ACP, acyclic hydrogenation product; DFP, defunctionalized product.

Table 5. Catalytic Data from Citral at 70 °C Transformations with 5 wt % Ni/H-β-38 and Different 11 wt % Ni-H-β-38-Bentonite Powder Catalysts[a]

catalyst	initial rate (mmol/(min·g_{Ni}))	citral conversion after 600 min (%)	$TOF_{menthol}$ (min^{-1})	S_{IP} (%)[b]	S_{Me} (%)[b]	S_{ACP} (%)[b]	S_{DFP} (%)[b]	$SterS_{ME}$ (%)[b]
5 wt % Ni/H-β-38	2.0	n.a.	n.d.	19[c]	0[c]	24[c]	57[c]	n.a.[c]
NiN	5.0	100	3.7×10^{-3}	21 (0)	38 (70)	36 (22)	6 (12)	64–70
NiA	6.0	100	0.5×10^{-3}	11 (3)	3 (58)	33 (22)	19 (24)	60–72
NiS	0.3	88	0.1×10^{-4}	11[d]	3[d]	37[d]	45[d]	n.a.
NiCl	0.2	91	n.d.	2 (1)	46 (48)	24 (23)	20 (20)	72

[a]A, acetate; C, chloride; N, nitrate; and S, sulfate. In Parenthesis, Values after 660 min. [b]Selectivity to isopulegols S_{IP}, menthols S_{Me}, acyclic hydrogenation products S_{ACP}, and defunctionalized products S_{DFP} and stereoselectivity to menthol $SterS_{ME}$ at 90% conversion,. [c]At 35% conversion. [d]After 516 min.

BAS = 156 μmol/g, total LAS = 74 μmol/g) (Table 3 entry 2). The NiN catalyst contains mainly weak and medium Brønsted acid sites (60 and 96 μmol/g, respectively, and 0.4 μmol/g strong BAS) (Table 3 entry 2), which are desired for maximizing menthol selectivity,[21] whereas no menthols were detected for an acidic Ni/H-Y-5.1 catalyst (BAS = 291 μmol/g, LAS = 165 μmol/g). It is also important to note that in the NiN catalyst, composed of both H-β-38 and bentonite clay, not only zeolite but also bentonite affects the final properties of the catalyst, as can be seen from Table 3. In this Ni-composite catalyst, the BAS/LAS ratio is decreased in comparison to the acidity of the support only, H-β-38+ bentonite (Table 3, entry 9). In addition, very small amounts of strong Lewis acid sites are present in the NiN composite catalyst. Furthermore, it should be noticed that the bentonite binder *per se* is not inert for cyclization of citronellal as reported for this reaction

https://doi.org/10.1021/acs.oprd.2c00337
Org. Process Res. Dev. 2023, 27, 295−310

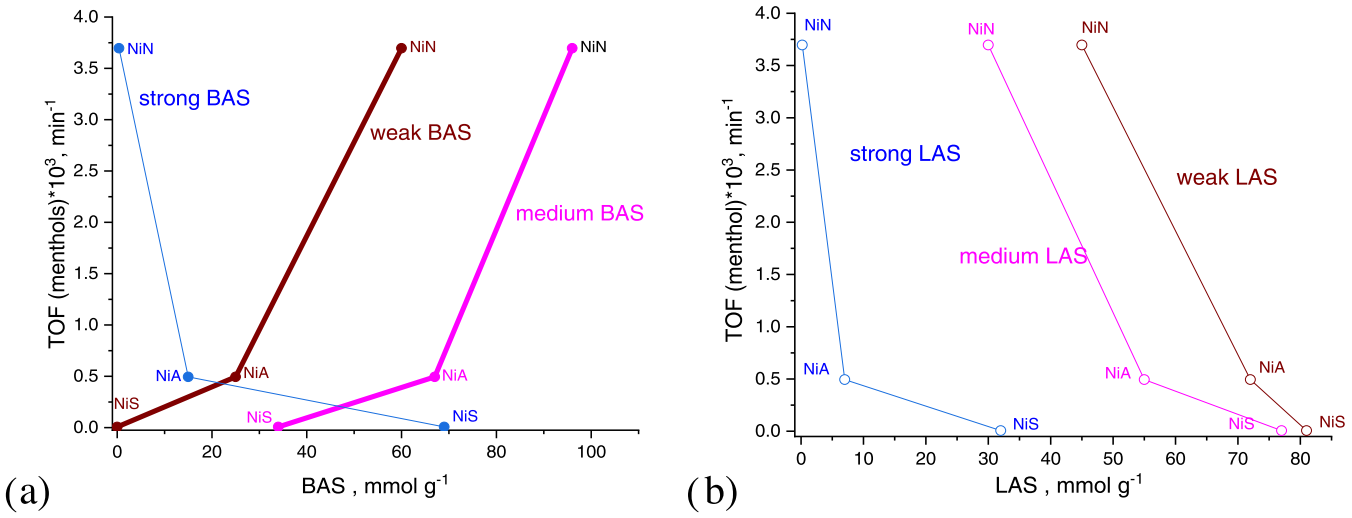

Figure 5. Dependence of TOF in menthol formation during citral hydrogenation over 11 wt % [(Ni-H-β-38)-bentonite] powder NiN, NiA, and NiS catalysts (data from Table 5) on the concentration of (a) BAS and (b) LAS of different strengths (data from Table 3). Reaction conditions are as in Figure 3.

conducted under 10 bar argon at 70 °C in a trickle-bed reactor.[19] In,[19] the yield of isopulegols was 23% at 53% conversion after 2 h time-on-stream. When comparing catalyst acidities, a mesoporous mildly acidic Ni/H-MCM-41 (BAS = 89 μmol/g, LAS = 168 μmolg/g) gave only ca. 2% yield of menthols at citral conversion below 40% at 70 °C and 10 bar H_2.[3] As a comparison, 94% yield of menthols was achieved in a batch reactor over a mildly acidic 8 wt % Ni/Al-MCM-41 catalyst at 20 MPa at 70 °C.[4] The main primary products over NiN and NiA are acyclic hydrogenation products, citronellol, and 3,7-dimethyloctanol, while the citronellol concentration is very low because it is very rapidly hydrogenated to 3,7-dimethyloctanol, indicating a high hydrogenating catalyst ability. The intermediate products, citronellal and pulegols, reacted rapidly further in the case of the NiN catalyst, with their yield exhibiting a maximum at 30 min. The menthol yield increased rapidly over this catalyst up to 180 min and remained constant thereafter. At the same time, the pulegol yield was already close to zero and a nearly complete citral conversion was reached. Furthermore, the yields of both acyclic hydrogenation products and defunctionalized products remained constant. On the other hand, for the second-best catalyst, NiA, the kinetic curves were quite analogous to those of NiN; however, the maximum yields of the intermediate products were obtained at 90 min instead of 30 min for NiN. This result can be explained by the egg-shell structure of the latter catalyst confirmed by HAADF-STEM-EDX (Figure S1), facilitating rapid hydrogenation reaction. The NiA catalyst also contained a much higher amount of strong Brønsted acid sites, which can promote formation of defunctionalized products (Table 3 entry 4 and Table 5). The NiCl catalyst exhibited a rather slow reaction rate due to the large Ni particle size. Thus, menthol formation started after 250 min, reaching a selectivity of 48% after 660 min. This catalyst, featured by a large amount of strong Brønsted acid sites, resulted in a high yield of defunctionalized products (Table 3 entry 5 and Table 5). Stereoselectivity to the desired menthol isomer varied for NiN and NiA in the range of 60−72% (Table 5). The worst performance was determined for the NiS catalyst, giving only traces of menthols (Table 5). Noteworthy is also that one of the main products was geraniol (Figure S5, Table S2), indicating that hydrogenation was retarded in the presence of sulfur and only 88% citral conversion was obtained after 660 min, while no menthol at all was produced.

Hydrogenation of citral over a microporous Ni/H-β-38 catalyst was also investigated, demonstrating that it was still exhibiting some activity for citral conversion as well as for hydrogenation and dehydration, as can be seen in Figure 4d. Formation of the defunctionalized products, namely, mentha-2,8-diene, p-mentha-1,3,8-triene, p-mentha-1,5,8-triene, and o-cymene, was very rapidly increasing with time; therefore, after 3 h, they became the major part of the reaction mixture. No menthols were formed over Ni/H-β-38 due to the low conversion of citral (<35%) and at the same time also due to a rather acidic support (BAS = 116 μmol/g, LAS = 198 μmol/g) (Table 3, entry 1).

Better mechanistic understanding of the catalytic activity related to menthol formation can be obtained based on the turnover frequency of menthol formation $TOF_{menthol}$, which takes into account the metal dispersion. The values of $TOF_{menthol}$ over Ni/H-β-38-bentonite catalysts prepared from different nickel precursors presented in Table 5 indicate that $TOF_{menthol}$ increased as follows: NiS ≪ NiA < NiN. For citral-to-menthol transformations, the ex-nitrate catalyst with the largest Ni particles displayed the highest TOF value. This is probably related to the easier adsorption of the intermediate isopulegol, originating from citronellal cyclization, on larger Ni particles in a flat mode. A similar behavior was observed for shape-selective hydrogenation of naphthalene over zeolite-supported Pt and Pd catalysts[40] or hydrogenation of other aromatics over Au-Pd/SiO_2-Al_2O_3 catalysts with different activities.[41,42] From Table 3, the acid site distribution of the catalysts from different precursors is similar, even if relatively large differences in the acid strength were observed. Considering the total acid site concentration (second to the last column in Table 3), it can be concluded that the observed catalyst acidity trend NiS > NiA > NiN is opposite to the order of activity expressed through $TOF_{menthol}$. However, a positive correlation between $TOF_{menthol}$ in menthol formation (Table 5) and the concentration of weak and medium-strong Brønsted acid sites (Table 3) follows from Figure 5. Interestingly, similar correlations of $TOF_{menthol}$ for strong BAS and all LAS of

https://doi.org/10.1021/acs.oprd.2c00337
Org. Process Res. Dev. 2023, 27, 295−310

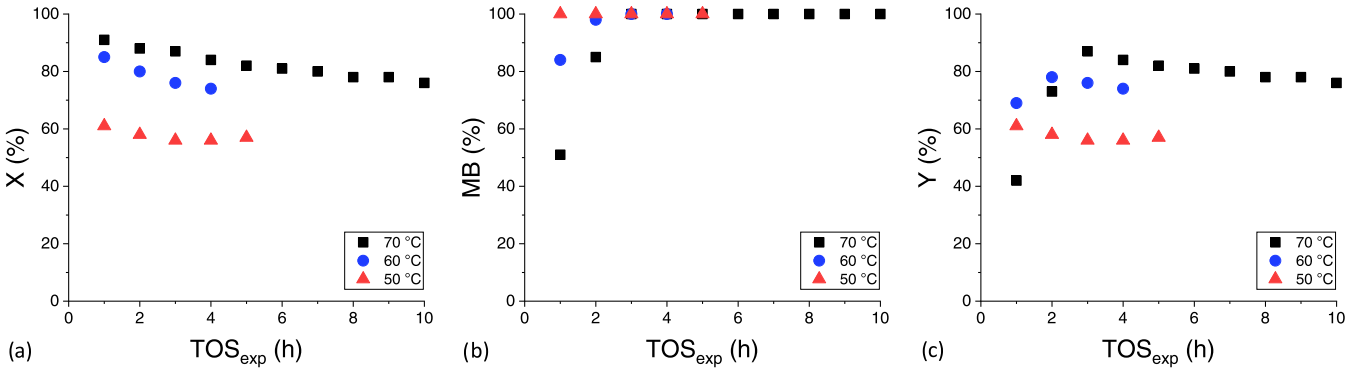

Figure 6. Transformation of citral in a trickle-bed reactor: (a) citral conversion, (b) liquid-phase mass balance closure, (c) total yield of the liquid-phase products as a function of time-on-stream. Conditions: 50−70 °C, 10 bar H_2, 0.3 mL/min feed, 0.09 M initial concentration of citral in cyclohexane, 1 g of catalyst, 5 wt % [(NiN/H-β-38) + bentonite], residence time of 12.5 min.

different strengths could not be seen. It seems thus that weak and medium-strong Brønsted acid sites are essential for menthol formation, accelerating probably not only citronellal cyclization, which is intuitively expected, but also hydrogenation of the double bonds. The hydrogenation activity enhancement in the presence of a mildly acidic support has been noticed already in hydrogenation of toluene.[41] It can be tentatively hypothesized that probably in addition to metal centers, the acid sites of the support might also play some role in double-bond hydrogenation as a consequence of hydrogen spillover.[43,44]

Activity and Selectivity of Ex-nitrate Ni Containing Extrudates in the Trickle-Bed Reactor. The experimental results obtained for citral transformations to menthol over 5 wt % ex-nitrate [(NiN/H-β-38) + bentonite] extrudates in a trickle-bed reactor at different temperatures of 50, 60, and 70 °C as a function of time-on-stream (TOS) are shown in Figure 6. The initial citral conversion was 60−90% (at 1 h of TOS) with the observed deactivation rate of ca. 2.7% per 1 h of TOS (Figure 6, Table 7). During these experiments, citral conversion decreased from 90 to 75% at 70 °C within 10 h TOS and from 60 to 55% at 50 °C in 5 h TOS. As expected, the citral conversion increased with increasing temperature from 50 to 70 °C. The *cis*-to-*trans* ratio increased slightly by a factor ranging from 1.0 to 1.2 when increasing the reaction temperature from 50 to 70 °C. According to the increasing values of the liquid-phase mass balance closure (MB) and the total yield of liquid-phase products (Y) with TOS it can be concluded that the steady state was achieved at ca. 3 h of TOS at all temperatures (Figure 6b,c). The highest total yield of the liquid-phase products of 87% was obtained at 70 °C in 3 h of TOS (Figure 6c).

Comparison of the performance of the [(Ni/H-β-38)+bentonite] composite catalyst with Ni/H-β-38 containing other clays as binders is shown in Table 8, where all catalysts are derived from the nitrate precursor. These results reveal that the catalyst deactivation rate was also the highest one among the studied extrudates in the case of [Ni/(H-β-38+sepiolite)], which exhibited the largest average Ni particle size. As a comparison with Ni-extrudates, a significantly faster initial deactivation rate of 9.3% per 1 h of TOS at 83% citral conversion over Ru extrudates was observed in[18] at 70 °C and 10 bar with the flow rate of the citral solution in cyclohexane being 0.4 mL/min over 1 g of Ru/H-MCM-41 extrudates with a bindzil binder (SiO_2). A significantly lower citral conversion of 44% with a similar initial deactivation rate of 11% per 1 h of TOS, as for Ru/H-MCM-41 extrudates, was obtained over a lower amount (0.7 g) of less acidic Ru/H-Y-80 extrudates with a bindzil binder under the same conditions.[17] This obviously indicates a higher stability of the Ni catalysts compared to the Ru counterparts in citral transformations. Note that the specific surface area of the [(NiN/H-β-38) + bentonite] extruded catalyst decreased by only 33% without changing the mesoporous structure after 19 h TOS (Table 2, entries 11, 12), demonstrating that introduction of bentonite promoted formation of mesopores beneficial for the liquid-phase hydrogenation.

The XRD analysis of the spent 5 wt % [(NiN/H-β-38) + bentonite] extrudates revealed that metallic nickel was preserved during the reaction and the H-β zeolite structure was intact (Figure 1b). The XRD pattern of the spent catalyst demonstrates reflexes similar to those of β-zeolite (PDF No. 00-056-0487) and Ni^0 (PDF No. 04-0850), with the calculated value of the lattice parameter a = 3.524 Å and average CSD size D_{Ni} = 18.0 nm. Characteristic reflexes from the NiO phase are not reliably observed but could be present in the sample because of the weak reflex at 2Θ = 43.3°. It indicates that the preliminary ex-nitrate catalyst reductive activation resulted in formation of Ni species predominantly in the metallic state that were maintained during citral hydrogenation without any noticeable change of the crystallographic Ni particle size. A similar metallic state of Ni was observed by XRD in the spent Ni/(H-β-38) extrudates prepared by shaping with sepiolite[22] and attapulgite,[23] indicating that formation of Ni^0 is independent of the inorganic clay binder type.

Possible metal leaching also was investigated by determining the Ni content in the fresh and spent catalysts with the ICP-OES method (Table 6). The results showed that almost no Ni leaching occurred from 5 wt % Ni/H-β-38 during 5 h, while minimum leaching was detected for [(Ni/H-β-38)+bentonite] extrudates during 10 h in a similar operation window, which could be expected due to mild reaction conditions.

Table 6. ICP-OES Results of the Fresh and Spent Catalysts[a]

catalyst		Ni (wt %)
5 wt % NiN/H-β-38 P	fresh	6.5
	spent	6.5
5 wt % (NiN/H-β-38) + bentonite E	fresh	5.4
	spent	5.0

[a]P, powder; E, extrudate.

https://doi.org/10.1021/acs.oprd.2c00337
Org. Process Res. Dev. 2023, 27, 295−310

The apparent activation energy was determined to be 18.6 kJ/mol (Figure 7). This is a smaller value in comparison with

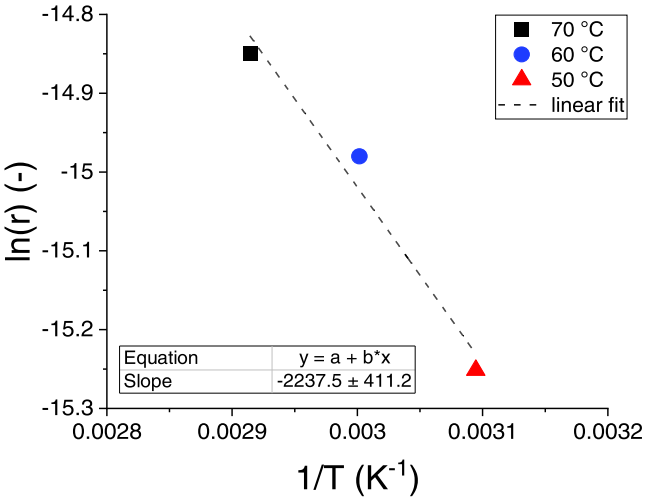

Figure 7. Natural logarithm of the reaction rate as a function of the reciprocal temperature. Conditions: 50−70 °C, 10 bar H_2, 0.3 mL/min feed, 0.09 M initial concentration of citral in cyclohexane, 1 g of catalyst, 5 wt % [(NiN/H-β-38) + bentonite], residence time of 12.5 min.

the value reported by Mäki-Arvela et al.[45] for the citral hydrogenation over the supported Pd-ionic liquid catalyst in the kinetic regime (70−130 °C, 20−40 bar, 0.5 g catalyst, 0.1 M citral in cyclohexane) being of 31 kJ/mol when the reaction order with respect to hydrogen was close to 1. Apparently, such results indicate the presence of mass transfer limitations in the case of extrudates.

To confirm the potential impact of mass transfer, the Weisz modulus was calculated for the experiment at 70 °C (Figure 6a) taking into account the fact that the surface concentration of citral corresponds to its bulk concentration at 80% conversion for an initial concentration of citral equal to 0.09 M. Considering the diffusion length of the catalyst particles as 0.3 mm and the effective diffusion coefficient of hydrogen equal to 10^{-9} m^2/s, the value of the Weisz modulus is ca. 3, significantly exceeding the minimum value (i.e., 0.6) for the first-order reaction.

Selectivity to different products as a function of conversion is depicted in Figure 8 and in Table 7. Initially, at 70 °C, a high amount of defunctionalized products (DFPs, including *p*-menthane, mentha-2,8-diene, and *p*-mentha-1,3,8-triene) (Scheme 1) was formed over [(Ni/H-β-38) + bentonite] extrudates, which exhibited a rather high BAS/LAS ratio of 0.9 (Table 3). Their selectivity, however, dropped substantially after 4 h time-on-stream when most acidic sites were deactivated. Thereafter, selectivities to menthol and hydrogenated acyclic products (ACPs) (Scheme 1) increased rapidly up to 44 and 28%, respectively. The maximum menthol selectivity was 45% at 70 °C, which decreased when the temperature decreased with increasing time-on-stream to 60 °C and finally to 50 °C. The final selectivities at 50 °C to menthols and acyclic hydrogenation products were 32 and 45%, respectively. As a comparison, only ca. 8−10% DFPs were formed during the whole 56 h experiment in a trickle-bed reactor over Ni supported on mesoporous alumina silicate-sepiolite extrudates, devoid of strong Brønsted acid sites.[2] This result suggests that strong Brønsted acid sites promote dehydration of menthols. Selectivity to acyclic hydrogenation products (ACPs), formed in the first step of transformation, decreased with increasing conversion. The reaction proceeded rapidly from citronellal to pulegols and menthols. At a higher temperature, formation of 3,7-dimethyloctanol was favored, while at 50 °C, increased amounts of citronellal were determined.

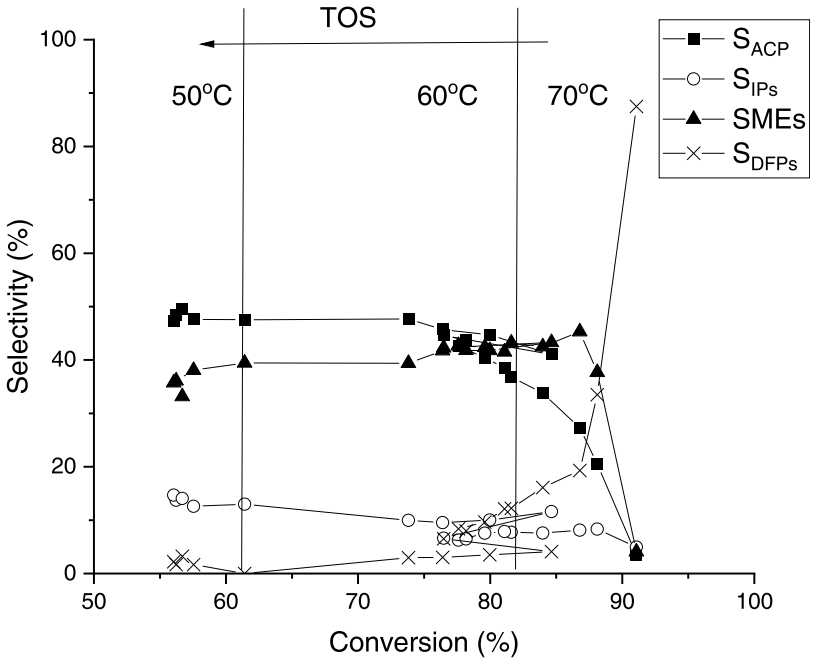

Figure 8. Selectivity to menthols, acyclic hydrogenation products, pulegols, and defunctionalized products as a function of conversion in citral transformations to menthol over 5 wt % [(NiN/H-β-38)+bentonite] extrudates. Time-on-stream (TOS) increases from the right to the left. Citral conversion increased when the temperature was changed from 70 to 60 °C.

https://doi.org/10.1021/acs.oprd.2c00337
Org. Process Res. Dev. 2023, 27, 295−310

Table 7. Selectivity (%) in Citral Transformations to Menthol over [Ni/(H-β-38+Bentonite)] Extrudates in 4 h of Time-on-Stream[a]

T	X	menthol isomers				SterS$_{MNT}$	isopulegol isomers			SterS$_{IP}$	acyclic hydrogenation products					defunctionalized products		
°C	%	MNT	NM	IM	NIM	%	IP	NIP	IIP	NIIP	%	DME	UNK	CAL	DMO	CLOL	NRL	pMA	M28D	138pMTE
50	56	23.9	8.2	1.5	2.2	67	7.9	4.6	0.0	2.2	54	0.0	2.0	31.7	13.0	2.7	0.0	0.2	0.0	0.0
60	74	26.3	10.0	0.7	2.3	67	5.6	3.7	0.0	0.7	56	0.0	0.0	28.3	17.2	2.1	0.0	0.0	3.0	0.0
70	84	29.8	9.4	0.7	2.5	70	4.4	2.4	0.0	0.8	58	0.6	2.4	14.0	18.1	0.8	0.3	8.1	3.5	2.1

[a]Conditions: 50−70 °C, 10 Bar H_2, 0.3 mL/min of Feed, 0.09 M Initial Concentration of Citral in Cyclohexane, 1 g of Catalyst, Residence Time of 12.5 min. Notation: T − Temperature, X − Citral Conversion, ME − Menthol Isomer, NME − Neomenthol Isomer, IME − Isomenthol Isomer, NIME − Neoisomenthol Isomer, IP − Isopulegol Isomer, NIP − Neoisopulegol Isomer, IIP − Isoisopulegol Isomer, NIIP − Neoisoisopulegol Isomer, DME - 2.6-Dimethyloctane, UNK − Unknown Compound, CAL − Citronellal, DMO − 3,7-Dimethyloctan-1-ol, CLOL − Citronellol, NRL − Nerol, pMA − p-Menthane, M28D − Mentha-2,8-diene, 138pMTE − p-Mentha-1,3,8-triene. SterS$_{IP}$ Denotes Stereoselectivity.

The highest yield of the desired menthols of 40% (maximum selectivity to menthols was 45%) was obtained with stereoselectivity to menthol of 70% at 70 °C. A higher menthol selectivity at 70 °C is expected because it has been observed that the activation energy for formation of IP is higher than that for hydrogenation products. The activation energy of 104 kJ/mol determined for citronellal cyclization[46] was higher than the activation energies for its hydrogenation to citronellol and dihydrocitronellal, being 72.7 and 79 kJ/mol, respectively. When comparing, however, the performance of three different extrudates (Table 8), it can be seen that at the same citral conversion level of 84% the menthol selectivity was the highest for [Ni/(H-β-38+sepiolite)] and [Ni/(H-β-38 + attapulgite)], which exhibited a lower BAS/LAS ratio. Stereoselectivity to the menthol isomer was slightly lower (67%) at 50 and 60 °C than at 70 °C (Table 7). Stereoselectivity to the isopulegol isomer marginally increased from 54% to 58% when the temperature was increased from 50 to 70 °C. Previously, stereoselectivities in citral transformations to menthols in a trickle-bed reactor over Ni/MAS-sepiolite, Ni/H-β-38-sepiolite, and Ni/H-β-38-attapulgite were 62−75,[2] 71−76,[21] and 68−75%,[22] respectively. Analogously similar stereoselectivity to the menthol isomer of 70% was only observed in the transient period (<2 h of TOS) for Ru/H-Y-80 extrudates at the maximum menthol yield of 6%.[17] As a comparison, after 3 h, a lower stereoselectivity to menthol isomer of ca. 50% was obtained at low menthol yields (below 2%) for Ru extrudates containing H-Y-80[17] or H-MCM-41[18] as supports and a bindzil binder (SiO_2) at 70 °C and 10 bar hydrogen.

Overall, for Ni/H-β-38 extrudates containing the bentonite clay binder, the major products were menthols followed by the acyclic hydrogenated products. On the contrary, for Ru extrudates containing the bindzil (silica) binder,[17,18] the major products were the defunctionalized compounds followed by isopulegols. Interestingly, it was observed in[18] over Ru extrudates that the product distribution varied when the same power and extrudate catalysts were investigated in batch and trickle-bed reactors, respectively. In the current case with [(Ni/H-β-38) + bentonite], the main product in both cases was the same, namely, menthol followed by acyclic hydrogenation products (compare Figure 8 at 70 °C and Table 5 for batch reactor results). On the other hand, in the current case, operation in a trickle-bed reactor promoted formation of more defunctionalized products than obtained in a batch reactor. It can be subsequently concluded that the metal has a significantly higher impact on the final selectivity to the desired product in continuous citral transformations in a trickle-bed reactor than acidity of the support or the binder.

CONCLUSIONS

One-pot catalytic synthesis of menthol from citral was investigated both in a batch and in a continuous reactor using a bifunctional Ni/H-β-38-bentonite composite. The catalyst synthesis was optimized by preparing the Ni/H-β-38-bentonite composite using different nickel salts as precursors, such as nickel nitrate, chloride, sulfate, and acetate, clearly showing how selection of a precursor can influence properties of nickel-containing catalysts. The most efficient catalyst was synthesized from nickel nitrate as a precursor, while the second-best catalyst was made from acetate, giving menthol isomer selectivities of 70 and 58%, respectively, at 70 °C under 10 bar total pressure. These results were correlated with the hydrogen temperature-programmed reduction data, showing

https://doi.org/10.1021/acs.oprd.2c00337
Org. Process Res. Dev. 2023, 27, 295−310

Table 8. Citral to Menthol Transformations over Extruded Ni-H-β-38 Catalysts with Different Clay Binders

catalyst	decrease of conversion with TOS (%/h)	TAS (μmol/$g_{cat.}$)	BAS/LAS	amount of strong BAS (μmol/$g_{cat.}$)	average Ni particle size (TEM) (nm)	S_{ME} (%) at 84% conversion[a]	refs
[(Ni/H-β-38) + bentonite]	2.7	273	0.9	4	11	40 (45)	current work
[Ni/(H-β-38 + sepiolite)]	3.3	230	0.6	21	19[b]	48 (45)	21
[Ni/(H-β-38 + attapulgite)]	2.4	222	0.4	35	10	53 (54)	22

[a]In parenthesis, the highest menthol selectivity. [b]Determined by XRD.

that both nickel nitrate and nickel acetate exhibiting lower decomposition temperatures are characterized by lower reduction temperatures compared to nickel sulfate and chloride counterparts. The temperature for maximum hydrogen consumption for these catalysts was rather low, i.e., 377 and 325 °C for nitrate and acetate, respectively, facilitating efficient Ni species reduction when the catalyst was reduced prior to the reaction at 450 °C. The average nickel particle sizes for nitrate and acetate catalysts were found to be 11 nm and 6 nm, respectively. These catalysts also possess a relatively low amount of strong Brønsted acid sites, whereas the weak and medium Brønsted acid sites are shown to be essential for menthol formation, accelerating both citronellal cyclization and hydrogenation of the double bonds.

The best nickel precursor nickel nitrate was used to prepare extrudates in which Ni was first loaded on H-β-38, followed by extrusion with bentonite. These extrudates were used as catalysts in one-pot transformations of citral to menthol in a trickle-bed reactor in the temperature range from 50 to 70 °C under 10 bar hydrogen. The determined apparent activation energy for citral transformation of 18.6 kJ/mol indicated the presence of mass transfer limitations. Some deactivation was visible as the citral conversion decreased from 90 to 75% at 70 °C during 10 h time-on-stream and from 60 to 55% at 50 °C within 5 h time-on-stream. Initially, at 70 °C, defunctionalized menthanes and menthenes were mainly produced; however, after 3 h time-on-stream, their selectivity dropped substantially when the most acidic sites were deactivated. Thereafter, selectivity to hydrogenated acyclic products increased rapidly up to 44% at 50 °C. The maximum menthol selectivity at 70 °C was initially 45%, and it decreased until 32% when the temperature was decreased to 50 °C. Performance of the ex-nitrate Ni-H-β-38-bentonite composite catalyst was comparable to that of the ex-nitrate Ni/H-β-38-sepiolite clay, giving about the same menthol selectivity of 45%. Deactivation of Ni-H-β-38 with bentonite as a binder was also similar to previously reported data for sepiolite and attapulgite clays. At the same time, a steady-state activity could be reliably reached after an initial period of deactivation, indicating that the scale-up of such catalysts could in fact be feasible.

This study, along with previous investigations for other clay binders, such as sepiolite and attapulgite for Ni-H-β-38 extrudates, allows concluding that a balanced ratio of the acid sites as well as a proper Ni precursor was beneficial for transformations of citral, elevating selectivity to menthol under optimized process parameters.

EXPERIMENTAL SECTION

Preparation of Ni Catalysts. The proton form H-β-38 was obtained from the commercial NH_4-β-38 zeolite (SiO_2/Al_2O_3 = 38, CP814C, Zeolyst International) by calcination during 50 min at 250 °C and 4 h at 400 °C (temperature ramp 4 °C/min). All solids were ground and dried overnight at 100 °C before using in the synthesis. A series of powdered 11 wt % Ni catalysts supported on a mixture of H-β-38 (SiO_2/Al_2O_3 = 38) zeolite and bentonite ($Al_2H_2O_6Si$, VWR International) (the mass ratio of zeolite/binder was 7:3) were prepared by wet impregnation with aqueous solutions of nickel nitrate $Ni(NO_3)_2{\cdot}6H_2O$ (CJSC Souzchimprom), nickel sulfate $Ni(SO_4)_2{\cdot}7H_2O$ (CJSC Souzchimprom), nickel acetate $Ni(CH_3COO)_2{\cdot}4H_2O$ (CJSC Souzchimprom), and nickel chloride $NiCl_2$ (CJSC Souzchimprom). The 11 wt % Ni-H-β-38-bentonite composites prepared from different precursors, such as nitrate, acetate, chloride, and sulfate, were denoted in this work as NiN, NiA, NiCl, and NiS, respectively. Powdered 5 wt % Ni catalyst supported on only H-β-38 (SiO_2/Al_2O_3 = 38) zeolite was prepared by wet impregnation of the zeolite with an aqueous solution of nickel nitrate $Ni(NO_3)_2{\cdot}6H_2O$ (CJSC Souzchimprom). After impregnation, all powdered samples were dried at 100 °C overnight in an oven and calcined for 6 h in a flow of air at 450 °C (temperature ramp 2 °C /min). Powdered Ni catalysts were preliminary reduced ex situ in hydrogen in two steps: 1 h at 250 °C (temperature ramp 2 °C/min) and then 4 h at 450 °C (temperature ramp 2 °C/min), cooled down to room temperature, flushed with nitrogen, and immersed in cyclohexane to avoid contact of Ni with air.

The 5 wt % Ni containing extrudates were prepared using H-β-38 (SiO_2/Al_2O_3 = 38) zeolite as an active phase, clay bentonite ($Al_2H_2O_6Si$, VWR International) as an inorganic binder, and methylcellulose (viscosity: 4000 cP, Sigma-Aldrich) as an organic binder to improve the rheological properties of the paste. The zeolite in the powder form was impregnated with the corresponding amount of an aqueous solution of nickel nitrate $Ni(NO_3)_2{\cdot}6H_2O$ (98%) (Sigma-Aldrich, >97%), followed by drying at 100 °C overnight and calcination at 450 °C for 6 h in a muffle oven to decompose the nickel nitrate. Thereafter, the zeolite containing NiO was mixed at room temperature with methylcellulose (1.0 wt %), the corresponding amount of bentonite (the mass ratio of zeolite/binder was 7:3), and distilled water to obtain an elastic paste for further extrusion into a cylindrical shape using a lab-scale extruder (TBL-2, Tianjin Tianda Beiyang Chemical Co. Ltd., China). The fabricated extrudates of 1.5 mm diameter were dried overnight at 100 °C, calcined at 500 °C for 4 h in a muffle oven, and cut to a length of ca. 0.6−1.0 cm. Before a catalytic run, the extrudates were reduced in situ in hydrogen at 350 °C for 2.5 h with a temperature ramp of 2 °C/min. In the current study, 5 wt % Ni containing extrudates were denoted as [Ni/(H-β-38) + bentonite]. For comparison, extrudates containing 5 wt % Ni were prepared by impregnating a mechanical mixture of H-β-38 and bentonite with the ratio of 7:3 with nickel nitrate similar to impregnation of only H-β-38 giving [Ni/(H-β-38)+bentonite]. Such a catalyst was denoted as [Ni/(H-β-38+bentonite)].

https://doi.org/10.1021/acs.oprd.2c00337
Org. Process Res. Dev. 2023, 27, 295−310

Characterization of Ni Catalysts. Fresh and spent extrudates were characterized by several physicochemical methods. The textural properties such as the specific surface area, porosity, and pore size distribution were measured with nitrogen physisorption using a Micromeritics 3Flex-3500 device. The concentration of Ni in the entire volume of extrudates was detected by inductively coupled plasma−optical emission spectrometry using a PerkinElmer Optima 5300 DV instrument. The metal particle size and their location in extruded catalysts were analyzed by transmission electron microscopy with a JEOL JEM-1400Plus. Powder XRD patterns were obtained on a Bruker D8 advance diffractometer (Cu Kα radiation, λ = 0.15418 nm) equipped with a LynxEye position-sensitive detector. The data were collected in the 2θ range of 5−65° with a step of 0.05° and a collection time of 3 s. Phase identification was performed using the ICDD PDF-2 database [Powder Diffraction File database PDF-2, International Centre for Diffraction Data, 2009]. The average crystallite size of different phases was calculated by the line-broadening analysis according to the Scherrer equation. The structure and microstructure of the catalyst samples with different Ni precursors were studied by high-resolution transmission electron microscopy (HRTEM) using a ThemisZ electron microscope (Thermo Fisher Scientific) with an accelerating voltage of 200 kV and a limiting resolution of 0.07 nm. In high-angle annular dark-field scanning transmission electron microscopy, inelastically scattered electrons are received at high angles using an annular dark-field detector.

Images were recorded using a Ceta 16 CCD matrix (Thermo Fisher Scientific). The device is equipped with a SuperX (Thermo Fisher Scientific) energy-dispersive characteristic X-ray spectrometer (EDX) with a semiconductor Si detector (an energy resolution of 128 eV), allowing one to perform energy-dispersive X-ray spectroscopy (EDX) simultaneously with HAADF-STEM. For HRTEM analysis, catalyst particles were uniformly deposited on a perforated carbon support attached to a copper grid using an ultrasonic disperser UZD-1UCH2.

The strength and concentration of Brønsted and Lewis acid sites were determined by Fourier transform infrared spectroscopy with pyridine as a probe molecule using an ATI Mattson FTIR Infinity series spectrometer. Acidity was calculated based on the area of the peaks at 1545 and 1452 cm^{-1}, corresponding to Brønsted and Lewis acidities and the molar extinction factor.[47] The mechanical strength of extrudates was measured by the crush test using two parallel-plate Lorentzen & Wetter devices. Details about used equipment and characterization methods have been reported in our previous publication.[23]

Ni dispersion (D%) in Ni/H-β-38-bentonite catalysts was calculated from the average metal particle sizes, d_{Ni} (nm), assuming spherical uniform particles using the following equation: $D(\%) = 97.1/d_{Ni}$.[48]

Catalytic Tests. The catalytic behavior of Ni containing extrudates was tested in continuous transformations of citral to menthol at 50−70 °C and 10 bar hydrogen in trickle-bed reactor conditions: 50−70 °C, 10 bar H_2, 0.3 mL/min feed, 0.09 M initial concentration of citral in cyclohexane, 1 g of catalyst, and residence time of citral solution in the catalyst bed of 12.5 min. For comparison, batch experiments over powder 5 wt % Ni/H-β-38 catalysts without a binder bentonite were performed with 0.2 g of catalyst and 0.09 M citral in cyclohexane under 70 °C and 10 bar hydrogen. Furthermore, to study the effect of the Ni precursor, a series of experiments were performed with different 11 wt % Ni-H-β-38-bentonite powder catalysts under the following conditions: before the reaction, the calcined catalysts (150 mg) were reduced under flowing H_2 in a U-tube reactor, flashed with N_2, and filled with 3 ml of cyclohexane in a N_2 flow. The suspension of the catalyst in cyclohexane was transferred into an autoclave, which was flashed with Ar during this transfer. A solution of citral (Aldrich, 95%, 205 mg) in 12 ml of cyclohexane was also loaded to the autoclave followed by sealing and flashing with H_2. The total liquid volume in the batch experiments was 15 ml, giving an initial citral concentration of 0.09 M.

To start the reaction, the temperature was increased to 70 °C and the pressure to 10.6 bar. The external and internal mass transfer limitations were suppressed by applying a high stirring speed (1000 rpm) and small catalyst particles (below 70 μm), respectively.

The liquid samples were diluted with cyclohexane and analyzed using an Agilent GC 6890 N with a DB-1 column (30 m × 250 μm × 0.5 μm) and a flame ionization detector. The temperature program was as follows: 110−130 °C (0.4 °C/min) and then 130−280 °C (13 °C/min, held 10 min). Details of the analysis and experimental setups have been provided in our previous publications.[2,21,22]

The turnover frequency, $TOF_{menthol}$ (min^{-1}), was calculated as a reaction rate r_i, i.e., number of menthol moles formed per min (mmol/min) calculated from the slope in the linear region of the formation of menthol vs time plots, per number of exposed metal atoms calculated from the molar content of metal n(Ni) (mmol) multiplied by dispersion D% using the following expression: TOF = r_i/n(Ni)D%. As mentioned above, the dispersion was determined from the average size of Ni particles according to the TEM measurements. Selectivity of a product i was calculated from $S = \frac{Y_i}{\sum Y} \times 100\%$, where Y_i is the yield of this product and the denominator contains yields of all products.

■ ASSOCIATED CONTENT

Supporting Information

The Supporting Information is available free of charge at https://pubs.acs.org/doi/10.1021/acs.oprd.2c00337.

Catalyst characterization: average mechanical strength of extrudates; catalytic data: chromatogram of the sample withdrawn from one-pot transformation of citral over the NiS catalyst; and GCMS identification of the products obtained over the NiS/H-β-38- bentonite catalyst (PDF)

■ AUTHOR INFORMATION

Corresponding Author

Dmitry Yu. Murzin − *Johan Gadolin Process Chemistry Centre, Åbo Akademi University, 20500 Turku/Åbo, Finland;* orcid.org/0000-0003-0788-2643; Email: dmurzin@abo.fi

Authors

Irina L. Simakova − *Boreskov Institute of Catalysis, 630090 Novosibirsk, Russia;* orcid.org/0000-0002-5138-4847

Zuzana Vajglová − *Johan Gadolin Process Chemistry Centre, Åbo Akademi University, 20500 Turku/Åbo, Finland*

Mark Martínez-Klimov − *Johan Gadolin Process Chemistry Centre, Åbo Akademi University, 20500 Turku/Åbo, Finland*

https://doi.org/10.1021/acs.oprd.2c00337
Org. Process Res. Dev. 2023, 27, 295−310

Kari Eränen − *Johan Gadolin Process Chemistry Centre, Åbo Akademi University, 20500 Turku/Åbo, Finland*
Markus Peurla − *Institute of Biomedicine, University of Turku, 20520 Turku, Finland*
Päivi Mäki-Arvela − *Johan Gadolin Process Chemistry Centre, Åbo Akademi University, 20500 Turku/Åbo, Finland;* orcid.org/0000-0002-7055-9358

Complete contact information is available at: https://pubs.acs.org/10.1021/acs.oprd.2c00337

Notes

The authors declare no competing financial interest.

■ ACKNOWLEDGMENTS

The authors are grateful to the Academy of Finland for funding through the project: One pot continuous transformation of citral to menthol, comprising hydrogenation and cyclization steps. Electron microscopy of samples was processed and analyzed at the Electron Microscopy Laboratory, Institute of Biomedicine, University of Turku, which receives financial support from Biocenter Finland. TEM and HAADF-STEM-EDX analyses were performed by Dr. E. Gerasimov (Boreskov Institute of Catalysis), and XRD analysis was done by V. Pakharukova (Boreskov Institute of Catalysis). I.S. is grateful for the support from the Ministry of Science and Higher Education of the Russian Federation under the governmental order for the Boreskov Institute of Catalysis (project AAAA-A21-121011390055-8).

■ REFERENCES

(1) Dylong, D. P.; Hausoul, J. C.; Palkovits, R.; Eisenacher, M. Synthesis of (−)-Menthol: Industrial Synthesis Routes and Recent Development. *Flavour Fragr. J.* **2022**, *37*, 195−209.
(2) Simakova, I. L.; Vajglová, Z.; Mäki-Arvela, P.; Eränen, K.; Hupa, L.; Peurla, M.; Mäkilä, E. M.; Wärnå, J.; Murzin, D. Y. Citral-to-Menthol Transformations in a Continuous Reactor over Ni/Mesoporous Aluminosilicate Extrudates Containing a Sepiolite Clay Binder. *Org. Process Res. Dev.* **2022**, *26*, 387−403.
(3) Makiarvela, P.; Kumar, N.; Kubicka, D.; Nasir, A.; Heikkilä, T.; Lehto, V.-P.; Sjöholm, R.; Salmi, T.; Murzin, D. Y. One-pot Citral Transformation to Menthol over Bifunctional Micro- and Mesoporous Metal Modified Catalysts: Effect of Catalyst Support and Metal. *J. Mol. Catal. A. Chem.* **2005**, *240*, 72−81.
(4) Trasarti, A. F.; Marchi, A. J.; Apesteguia, C. R. Design of Catalyst Systems for the One-Pot Synthesis of Menthols from Citral. *J. Catal.* **2007**, *247*, 155−165.
(5) Negoi, A.; Teinz, K.; Kemnitz, E.; Wuttke, S.; Parvulescu, V. I.; Coman, S. M. Bifunctional Nanoscopic Catalysts for the One-Pot Synthesis of (±)-Menthol from Citral. *Top. Catal.* **2012**, *55*, 680−687.
(6) Shah, A. K.; Maitlo, G.; Shah, A. A.; Channa, I. A.; Kandhro, G. A.; Maitlo, H. A.; Bhatti, U. H.; Shah, A.; Memon, A. Q.; Jatoi, A. S.; Park, Y. H. One Pot Menthol Synthesis via Hydrogenations of Citral and Citronellal over Montmorillonite-Supported Pd/Ni-Heteropolyacid Bifunctional Catalysts. *React. Kin. Mech. Catal.* **2019**, *128*, 917−934.
(7) Chuah, G. K.; Liu, S. H.; Jaenicke, S.; Harrison, L. J. Cyclisation of Citronellal to Isopulegol Catalysed by Hydrous Zirconia and Other Solid Acids. *J. Catal.* **2001**, *200*, 352−359.
(8) Álvarez-Rodríguez, J.; Cerro-Alarcon, M.; Guerrero-Ruiz, A.; Rodrıguez-Ramos, I.; Arcoya, A. Effect of Nickel Precursor and the Copper Addition on the Surface Properties of Ni/KL-Supported Catalysts for Selective Hydrogenation of Citral. *Appl. Catal., A* **2008**, *348*, 241−250.
(9) Kocer, T.; Saraç-Öztuna, F. E.; Kurtoglu-Öztulum, S. F.; Unal, U.; Uzun, A. Effect of Nickel Precursor on the Catalytic Performance of Graphene Aerogel-Supported Nickel Nanoparticles for the Production of COx-free Hydrogen by Ammonia Decomposition. *Energy Technol.* **2022**, *10*, No. 2100794.
(10) Wen, X.; Xu, L.; Chen, M.; Shi, Y.; Lv, C.; Cui, Y.; Wu, X.; Cheng, G.; Wu, C.; Miao, Z.; Wang, F.; Hu, X. Exploring the Influence of Nickel Precursors on Constructing Efficient Ni-Based CO_2 Methanation Catalysts Assisted with In-Situ Technologies. *Appl. Catal., B* **2021**, *297*, No. 120486.
(11) Wei, L.; Haije, W.; Kumar, N.; Peltonen, J.; Peurla, M.; Grenman, H.; de Jong, W. Influence of Nickel Precursors on The Properties and Performance of Ni Impregnated Zeolite 5A and 13X Catalysts in CO_2 Methanation. *Catal. Today* **2021**, *362*, 35−46.
(12) Jia, W.; Huang, X.; Yang, X.; Liu, X.; Cao, P.; Zhu, Z. Synergistic Roles of Surface Acidity and Ni Species in NiF_2/AlF_3 Catalysts for Pyrolysis of 1,1,1,2-Tetrafluoroethane. *Mol. Catal.* **2022**, *527*, No. 112433.
(13) Di Giuliano, A.; Gallucci, K.; Foscolo, P. U.; Courson, C. Effect of Ni Precursor Salts on Ni-Mayenite Catalysts for Steam Methane Reforming and on Ni-CaO-mayenite Materials for Sorption Enhanced Steam Methane Reforming. *Int. J. Hydrogen Energy* **2019**, *44*, 6461−6480.
(14) Wu, G.; Zhang, C.; Li, S.; Han, Z.; Wang, T.; Ma, X.; Gong, J. Hydrogen Production via Glycerol Steam Reforming over Ni/Al_2O_3: Influence of Nickel Precursors. *ACS Sustainable Chem. Eng.* **2013**, *1*, 1052−1062.
(15) Romero, M. D.; Calles, J. A.; Rodrıguez, A. Influence of the Preparation Method and Metal Precursor Compound on the Bifunctional Ni/HZSM-5 Catalysts. *Ind. Eng. Chem. Res.* **1997**, *36*, 3533−3540.
(16) Eliche-Quesada, D.; Merida-Robles, J.; Maireles-Torres, P.; Rodrıguez-Castellon, E.; Jimenez-Lopez, A. Hydrogenation and Ring Opening of Tetralin on Supported Nickel Zirconium-Doped Mesoporous Silica Catalysts. Influence of the Nickel Precursor. *Langmuir* **2003**, *19*, 4985−4991.
(17) Vajglová, Z.; Navas, M.; Mäki-Arvela, P.; Eränen, K.; Kumar, N.; Peurla, M.; Murzin, D. Y. Transformations of Citral over Bifunctional Ru-H-Y-80 Extrudates in a Continuous Reactor. *Chem. Eng. J.* **2022**, *429*, No. 132190.
(18) Vajglová, Z.; Mäki-Arvela, P.; Eränen, K.; Kumar, N.; Peurla, M.; Murzin, D. Y. Catalytic Transformations of Citral in a Continuous Flow over Bifunctional Ru-MCM-41 Extrudates. *Catal. Sci. Technol.* **2021**, *11*, 2873−2884.
(19) Vajglová, Z.; Simakova, I. L.; Eränen, K.; Mäki-Arvela, P.; Kumar, N.; Peurla, M.; Tolvanen, S.; Efimov, A.; Hupa, L.; Peltonen, J.; Murzin, D. Y. The physicochemical and catalytic properties of clay extrudates in cyclization of citronellal. *Appl. Catal., A* **2022**, *629*, No. 118426.
(20) Zhao, S.; Collins, D.; Wang, L.; Huang, J. Influence of ZSM-5 Porosity and Binder Introduction on the Coke Formation in the Cracking of 1, 3, 5-Triisopropylbenzene. *Catal. Today* **2021**, *368*, 211−216.
(21) Mendes, P. S.; Silva, J. M.; Ribeiro, M. F.; Daudin, A.; Bouchy, C. From Powder to Extrudate Zeolite-Based Bifunctional Hydroisomerization Catalysts: on Preserving Zeolite Integrity and Optimizing Pt Location. *J. Ind. Eng. Chem.* **2018**, *62*, 72−83.
(22) Simakova, I.; Mäki-Arvela, P.; Martinez-Klimov, M.; Muller, J.; Vajglová, Z.; Peurla, M.; Eränen, K.; Murzin, D. Y. Continuous Synthesis of Menthol from Citronellal and Citral over Ni-Beta-Zeolite-Sepiolite Composite Catalyst. *Appl. Catal., A* **2022**, *636*, No. 118586.
(23) Simakova, I. L.; Mäki-Arvela, P.; Martínez-Klimov, M.; Muller, J.; Vajglová, Z.; Peurla, M.; Eränen, K.; Murzin, D. Y. One-Pot Synthesis of Menthol Starting from Citral over Ni Supported on Attapulgite-H-Beta-38 Extrudates in a Continuous Flow: Effect of Metal Location. *Ind. Eng. Chem. Res.* **2022**, *61*, 12998−13010.
(24) Lari, G. M.; de Moura, A. B.; Weimann, L.; Mitchell, S.; Mondelli, C.; Pérez-Ramírez, J. Design of a Technical Mg−Al Mixed Oxide Catalyst for the Continuous Manufacture of Glycerol Carbonate. *J. Mater. Chem. A* **2017**, *5*, 16200−16213.

(25) Oliveira, C. I. R. d.; Rocha, M. C.; Da Silva, A. L. N.; Bertolino, L. C. Characterization of Bentonite Clays from Cubati, Paraíba (Northeast of Brazil). *Cerâmica* **2016**, *62*, 272−277.
(26) Bertagnolli, C.; Kleinübing, S. J.; Da Silva, M. G. C. Preparation and Characterization of a Brazilian Bentonite Clay for Removal of Copper in Porous Beds. *Appl. Clay Sci.* **2011**, *53*, 73−79.
(27) Zaitan, H.; Bianchi, D.; Achak, O.; Chafik, T. A Comparative Study of the Adsorption and Desorption of O-Xylene onto Bentonite Clay and Alumina. *J. Hazard. Mater.* **2008**, *153*, 852−859.
(28) Baudouin, D.; Rodemerck, U.; Krumeich, F.; de Mallmann, A.; Szeto, K. C.; Ménard, H.; Veyre, L.; Candy, J.-P.; Webb, P. B.; Thieuleux, C.; Copéret, C. Particle Size Effect in the Low Temperature Reforming of Methane by Carbon Dioxide on Silica-Supported Ni Nanoparticles. *J. Catal.* **2013**, *297*, 27−34.
(29) Solkina, Y. S.; Reshetnikov, S. I.; Estrada, M.; Simakov, A.; Murzin, D. Y.; Simakova, I. L. Evaluation of Gold on Alumina Catalyst Deactivation Dynamics During α-Pinene Isomerization. *Chem. Eng. J.* **2011**, *176−177*, 42−48.
(30) Kubicka, D.; Kumar, N.; Venäläinen, T.; Karhu, H.; Kubickova, I.; Österholm, H.; Murzin, D. Y. The Metal-Support Interactions in Zeolite-Supported Noble Metals: the Influence of Metal Crystallites on the Support Acidity. *J. Phys. Chem. B* **2006**, *110*, 4937−4946.
(31) Villegas, J. I.; Kumar, N.; Heikkilä, T.; Lehto, V.-P.; Salmi, T.; Murzin, D. Y. Isomerization of *n*-Butane to Isobutane over Pt-modified Beta and ZSM-5 Zeolite Catalysts: Catalyst Deactivation and Regeneration. *Chem. Eng. J.* **2006**, *120*, 83−89.
(32) Wang, X.; Su, X.; Zhang, Q.; Hu, H. Effect of Additives on Ni-Based Catalysts for Hydrogen-Enriched Production from Steam Reforming of Biomass. *Energy Techn.* **2020**, *8*, No. 2000136.
(33) Kobayashi, Y.; Horiguchi, J.; Kobayashi, S.; Yamazaki, Y.; Omata, K.; Nagao, D.; Konno, M.; Yamada, M. Effect of NiO content in Mesoporous NiO-Al_2O_3 Catalysts for High Pressure Partial Oxidation of Methane to Syngas. *Appl. Catal., A* **2011**, *395*, 129−137.
(34) Fúnez, A.; De Lucas, A.; Sánchez, P.; Ramos, M. J.; Valverde, J. L. Hydroisomerization in Liquid Phase of a Refinery Naphtha Stream over Pt−Ni/H-Beta Zeolite Catalysts. *Chem. Eng. J.* **2008**, *136*, 267−275.
(35) Dollimore, D.; Pearce, J. Changes in the Surface Characteristics of Residues from the Thermal Decomposition of Nickel Oxysalts. *J. Thermal Anal.* **1974**, *6*, 321−333.
(36) Patil, P. S.; Kadam, L. D. Preparation and Characterization of Spray Pyrolyzed Nickel Oxide (NiO) Thin Films. *Appl. Surf. Sci.* **2002**, *199*, 211−221.
(37) Brockner, W.; Ehrhardt, C.; Gjikaj, M. Thermal Decomposition of Nickel Nitrate Hexahydrate, $Ni(NO_3)_2{\cdot}6H_2O$, in comparison to $Co(NO_3)_2{\cdot}6H_2O$ and $Ca(NO_3)_2{\cdot}4H_2O$. *Thermochim. Acta* **2007**, *456*, 64−68.
(38) Mohamed, M. A.; Halawy, S. A.; Ebrahim, M. M. Non-isothermal Decomposition of Nickel Acetate Tetrahydrate. *J. Anal. Appl. Pyrol.* **1993**, *27*, 109−110.
(39) Vajglova, Z.; Kumar, N.; Mäki-Arvela, P.; Eränen, K.; Peurla, M.; Hupa, L.; Nurmi, M.; Toivakka, M.; Murzin, D. Y. Synthesis and Physicochemical Characterization of Shaped Catalysts of Beta and Y Zeolites for Cyclization of Citronellal. *Ind. Eng. Chem. Res.* **2019**, *58*, 18084−18096.
(40) Schmitz, A. D.; Bowers, G.; Song, C. Shape-selective Hydrogenation of Naphthalene over Zeolite-Supported Pt and Pd Catalysts. *Catal. Today* **1996**, *31*, 45−56.
(41) Venezia, A. M.; Parola, V. L.; Pawelec, B.; Fierro, J. L. G. Hydrogenation of Aromatics over Au-Pd/SiO_2-Al_2O_3 Catalysts; Support Acidity Effect. *Appl. Catal., A* **2004**, *264*, 43−51.
(42) Hoyos, L. J.; Primet, M.; Praliaud, H. Sulfur Poisoning and Regeneration of Palladium-Based Catalysts. Part 1.-Dehydrogenation of Cyclohexane on Pd/Al_2O_3 and Pd/SiO_2−Al_2O_3 Catalysts. *J. Chem. Soc. Faraday Trans.* **1992**, *88*, 113−119.
(43) Poondi, D.; Vannice, M. A. Competitive Hydrogenation of Benzene and Toluene on Palladium and Platinum Catalysts. *J. Catal.* **1996**, *161*, 742−751.
(44) Chou, P.; Vannice, M. A. Benzene Hydrogenation over Supported and Unsupported Palladium: II. Reaction Model. *J. Catal.* **1987**, *107*, 140−153.
(45) Mäki-Arvela, P.; Mikkola, J. P.; Virtanen, P.; Karhu, H.; Salmi, T.; Murzin, D. Y.Supported Ionic Liquid Catalyst (SILCA) in the Hydrogenation of Citral. In *Studies in Surface Science and Catalysis*, Elsevier, 2006; Vol. *162*, pp 87−94.
(46) Plößer, J.; Lucas, M.; Wärnå, J.; Salmi, T.; Murzin, D. Y.; Claus, P. Kinetics of the One-Pot Transformation of Citronellal to Menthols on Ru/H-BEA Catalysts. *Org. Process Res. Dev.* **2016**, *20*, 1647−1653.
(47) Emeis, C. A. Determination of Integrated Molar Extinction Coefficients for Infrared Absorption Bands of Pyridine Adsorbed on Solid Acid Catalysts. *J. Catal.* **1993**, *141*, 347−354.
(48) Bartholomew, C. H.; Pannell, R.; Butler, J. L. Support and Crystallite Size Effects in CO Hydrogenation on Nickel. *J. Catal.* **1980**, *65*, 335−347.

https://doi.org/10.1021/acs.oprd.2c00337
Org. Process Res. Dev. 2023, 27, 295−310